Journal of Marine Research, 51, 697–736, 1993

Journal of
MARINE RESEARCH

Volume 51, Number 4

Deep circulation in the tropical North Atlantic

by Marjorie A. M. Friedrichs[1] and Melinda M. Hall[1]

ABSTRACT

A transatlantic CTD/ADCP (Conductivity, Temperature, Depth/Acoustic Doppler Current Profiler) section along 11N, taken in March 1989, has been used to compute geostrophic velocities; geostrophic transport is required to balance *in situ* values of the Ekman and shallow boundary current transports. The horizontal flow structure is described for eight layers, with particular emphasis on deep and bottom waters (four layers below $\theta = 4.7°C$). In the shallow layers, total North Brazil Current (NBC) transport agrees with other observations previously made in the month of March, while net northward flow of these layers across the western basin is also consistent with recent observations to the north. For each of the four deep layers, circulation patterns are illustrated by means of schematic cartoons. Each of these layers flows southward in the Deep Western Boundary Current, which has a magnitude of 26.5 Sv. Roughly half of this flow returns northward to the west of the Mid-Atlantic Ridge, confirming the existence of a hypothesized cyclonic recirculation gyre in the western basin of the tropical Atlantic. To varying degrees the deep and bottom waters also circulate cyclonically in the eastern basin, with net northward flow across this basin.

Partly as a result of the unusual appearance of the North Equatorial Countercurrent in March 1989, the *in situ* values of the meridional overturning cell (5.2 Sv), heat flux (3.0×10^{14} W), and freshwater flux (−0.65 Sv) computed from the 11N section depart significantly from estimates of these quantities in the literature. By forcing the 11N geostrophic velocities to balance annual average Ekman and NBC transports, annual average values of these fluxes (12 Sv; 11×10^{14} W; −0.6 Sv) are obtained, and are shown to agree well with historical estimates.

1. Introduction

It has become popular over the last 15 to 20 years to diagnose the large-scale meridional ocean circulation using long zonal hydrographic sections, ideally reaching

1. Physical Oceanography Department, Woods Hole Oceanographic Institution, Woods Hole, Massachusetts, 02543, U.S.A.

from one continental boundary to another. Earlier studies in the Atlantic have been based primarily on the International Geophysical Year (IGY) data (Fuglister, 1957); however, several zonal (and meridional) CTD/hydrographic/ADCP sections carried out in the last decade have allowed a more detailed look at the circulation, given the substantial improvement in both horizontal and vertical resolution. In this era of climate-conscious research, the analysis of such sections has proven to be a powerful tool for direct determination of ocean heat and freshwater fluxes (Hall and Bryden, 1982; Georgi and Toole, 1982; Roemmich, 1983; Wunsch, 1984; Bryden *et al.,* 1991; and others). In addition, however, careful cross-examinations of numerous data sets have revealed a level of complexity in the circulation not previously suspected, including an almost ubiquitous tendency toward recirculation gyres in the deep water (Schmitz and McCartney, 1993).

Historically the mid-latitude North Atlantic has been much better sampled than the tropics, thus leading to an advanced understanding of the circulation there; however, a recent wealth of hydrographic, float, and moored data nearer to the equator is revealing heretofore unrecognized complexities in the tropical Atlantic circulation as well. These include evidence for recirculation components in different strata of the deep flow (Molinari *et al.,* 1992; McCartney, 1993), the presence of strong time variability in the Deep Western Boundary Current (DWBC) (Johns *et al.,* 1993), and an indication that water parcels in the DWBC do not always pass directly into the South Atlantic, but instead are sometimes diverted a long distance eastward along the equator (Richardson and Schmitz, 1993).

In this work, we use a recent hydrographic section along 11N (nominal) to examine the large-scale meridional circulation in the tropical Atlantic, with particular emphasis on the recirculations of the deep flow. Reference levels for calculating geostrophic velocities have been chosen using weak integral constraints on the deep mass transport and concurrent estimates of the Ekman transport. We note here that the tropical North Atlantic is complicated by strong seasonal variability of the winds (and resulting Ekman transport) and of the North Brazil Current (NBC). Although we expect the baroclinic structure of the intermediate, deep, and bottom waters to be relatively independent of the Ekman and western boundary current transports, the meridional overturning cell (and hence the heat and freshwater fluxes) will depend on these factors.

This paper is organized as follows. In Section 2 we briefly describe the data, review historical reference level choices for this area, and survey the options for computing geostrophic transports. Based on this discussion, and balancing net mass, we argue for different reference levels in four distinct flow regimes across the 11N section. Section 3 then presents the net transports and horizontal circulation patterns that result for four shallow (above 1000 m) and four deep (below 1000 m) water mass layers. Particular attention is given to the latter, for which we include schematic cartoons of the flow. Section 4 focuses on the implied meridional overturning cell

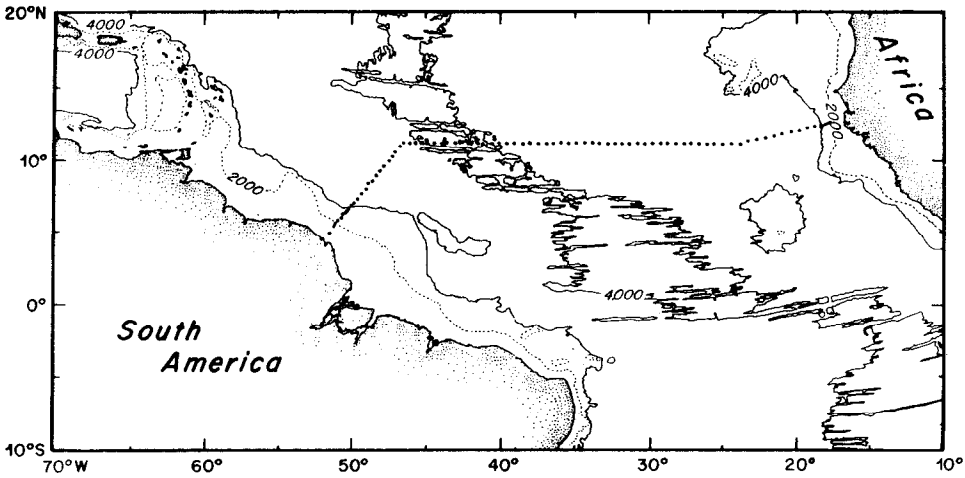

Figure 1. Cruise track of the 11N section in the tropical Atlantic. Individual dots denote locations of the 85 CTD's.

strength; for completeness, the associated heat and freshwater fluxes are computed. Recognizing the sensitivity of these fluxes to changes in the Ekman and western boundary current transports, we examine the impacts of such sources of uncertainty on the calculation. Finally, Section 5 recaps the salient issues of the paper, and points towards unanswered questions that are currently under investigation.

Because we realize that the paper is long, we note that the reference level choices and net mass balance are summarized at the end of Section 2, so that the reader may wish to skip directly to Section 3. Similarly, the discussion in Section 4 (meridional transports) may be understood independently of the results in Section 3 (horizontal circulation patterns).

2. Data and analysis techniques

In March 1989, the R.V. *Oceanus* occupied a CTD/hydrographic/ADCP zonal section across the tropical North Atlantic Ocean (D. Roemmich, M. Hall and T. Chereskin as co-PI's), repeating the track of a basin-wide deployment of SOFAR (Sound Fixing And Ranging) floats completed by P. Richardson and W. Schmitz the previous month. The 4000 km cruise track, shown in Figure 1, consisted of 85 CTD casts extending from the surface down to within 10 m of the bottom, and including 24 bottle samples analyzed for salinity, oxygen, and nutrients. Nominal station spacing over flat topography was 50 km, with shorter spacing of 15–25 km near coasts and in regions of strongly variable topography. Beginning at the 200 m isobath off Senegal, the ship angled slightly southwestward for a short segment before heading due west along 11 12 N. In order to approach the South American continental slope perpendicularly, the ship made another dogleg toward the southwest beginning at roughly

46.5W. Station 84 was located near the 200 m isobath off French Guiana. Westward of this cast, absolute velocities recorded by the ADCP (used in bottom-tracking mode) showed the presence of the strong NBC over the wide shallow shelf. The final cast (station 85) was taken on the continental shelf (60 m depth) and was located 57 km to the southwest of station 84.

One motivation for coordinating this cruise with the SOFAR float deployment was to examine the possibility of combining the float velocities in a sensible way with the ADCP velocities and hydrographic data in order to come up with a "best" determination of the absolute velocity field; however, due to the different nature of these measurements, it is not clear *a priori* how to make such a synthesis. On the other hand, the traditional method of choosing a reference level based primarily on water mass distributions has proven successful in many analyses of such long zonal (or meridional) sections. Inverse methods essentially quantify these choices, and demand that the resultant circulation satisfy certain constraints. With a single tropical Atlantic section, however, it is not feasible to prescribe conservation of mass transport in many density layers (a common approach in inverse modeling), since important water mass conversions occur in the North Atlantic. Our approach might be regarded as the first iteration in an inverse calculation subject to a minimal set of requirements suggested by the data and by what is already known regarding the Atlantic circulation. Future inversions seeking to refine details of the circulation (by including additional information) might profitably adopt our velocity field as their initial condition.

a. Ekman and shallow western boundary transport. Before detailing our reference level choices, we address the issue of balancing the net mass transport across the section, which demands knowledge of the Ekman and NBC transports. As noted in the introduction, total meridional transports of different water masses across the section depend on how we make these choices of Ekman and boundary current transports. The strong seasonal variability characteristic of these flows presents a philosophical difficulty. Should our final circulation patterns be interpreted as a synoptic realization of the flow? Are the patterns representative for the month of March in general? Or should the baroclinic structure be used with annual means of Ekman and boundary current transports to deduce a "climatological average" view of the circulation at 11N? For describing the circulation patterns, we adopt the first of these interpretations, i.e. that the results apply particularly to March, 1989; this choice circumvents the possibility that the gross baroclinic structure has strong seasonal (or other) variability. In Section 4, however, we explore the implications of the latter two approaches, particularly their effect on the heat and freshwater fluxes.

In the tropics, meridional Ekman transport is 2 to 3 times as large as in mid-latitudes (Roemmich, 1983) and is thus a major component of the meridional circulation. Chereskin and Roemmich (1991) have computed the Ekman transport

across our 11N transect (between stations 1 and 84) using three different methods. Assuming an Ekman depth of 100 m, they evaluated the difference between the geostrophic shear and the shear measured by the ADCP data to obtain a value of 12.0 ± 5.5 Sv, which agrees within error bars with that estimated from the shipboard winds, 8.8 ± 1.9 Sv. For comparison, they used the mean winds of Hellerman and Rosenstein (1983) for the month of March to obtain a third estimate of 13.5 ± 0.3 Sv. The lower values evaluated from the *in situ* data can be attributed to the relatively low winds experienced during the cruise period. Since we wish to represent the March 1989 circulation, we assume an Ekman transport of 9.1 ± 1.8 Sv, the mean of the two *in situ* estimates inversely weighted by their variance.

Along the western boundary of the transect, a strong northwestward flow of order 1 m s^{-1} was observed by the ADCP (in bottom tracking mode) to extend across the wide shallow shelf inshore of station 84 (Chereskin and Roemmich, 1991). Chereskin (pers. comm.) has calculated the transport of this flow. Absolute velocities were integrated from the bottom to 30 m (2.7 Sv), and a slab extrapolation was applied between 30 m and the surface (1.8 Sv), thus yielding 4.5 ± 1.0 Sv. Of this total transport, 3.3 Sv occurred in water depths of less than 100 m, in good agreement with the corresponding 3 Sv shallow NBC transport obtained by Candela *et al.* (1992) using ADCP and CTD data from March 1990. This shelf flow constitutes only a portion of the total NBC transport, which extended offshore through the last several CTD casts, where its transport is included in the geostrophic calculation. For clarity, we refer to the directly measured part of the current inshore of the 200 m isobath as the "shallow NBC."

Since at lowest order we demand that there be no net mass transport across 11N, in the remaining calculations we assume that the geostrophic component of the flow must balance the sum of the net northward Ekman transport and the shallow western boundary transport, i.e. 13.6 ± 2.1 Sv. Error bars on the geostrophic transports will include the propagation of the uncertainty in this sum.

b. Reference levels. Selecting a reference level of no motion is a fundamental aspect of our transport analysis. It is common practice to choose reference levels based on observed property distributions, which tend to be signatures of water masses of northern or southern origin. The underlying assumption is of course that waters of northern origin penetrate southward, and vice versa: for example, the boundary between North Atlantic Deep Water (NADW) and Antarctic Bottom Water (AABW) in principle should be a level of zero meridional velocity. The 11N section is particularly rich in overlapping strata of distinct water masses, identified in Table 1 by potential temperature ranges (also see Fig. 2b). At the bottom, AABW ($\theta < 1.8$°C) is identifiable by its high silicate content and low salinity relative to the overlying NADW (Fig. 2c,e). The latter, which occupies most of the deep water column (roughly 1000–4000 m depth), is a relatively high oxygen and high salinity water mass

Table 1. Definitions of water masses in terms of potential temperature classes.

surface water	$\theta > 24°C$
thermocline water	$12° < \theta < 24°C$
lower thermocline water	$7° < \theta < 12°C$
AAIW	$4.7° < \theta < 7.0°C$
upper NADW	$3.2° < \theta < 4.7°C$
middle NADW	$2.4° < \theta < 3.2°C$
lower NADW	$1.8° < \theta < 2.4°C$
AABW	$\theta < 1.8°C$

(Fig. 2c,d), and may be subdivided into three layers ($1.8° < \theta \leq 2.4°C$; $2.4° < \theta \leq 3.2°C$; $3.2°C < \theta \leq 4.7°C$). Centered at roughly 800 m depth is Antarctic Intermediate Water (AAIW, $4.7° < \theta \leq 7.0°C$), associated with another relative salinity minimum and increasing silicates (Fig. 2c,e). Overlying the AAIW are thermocline and surface waters, which we divide into three temperature classes following Schmitz and Richardson (1991). Although we do not discuss complexities in the circulation for waters with $\theta > 4.7°C$, Schmitz and Richardson (1991) have shown that these different layers probably are alternately of Northern and Southern Atlantic "origin."

In past hydrographic studies of the tropical Atlantic, historical precedence exists for applying either (1) a deep reference level (the boundary between lower NADW and AABW, roughly 4500 db, or $\theta \approx 1.8° - 1.9°C$; Whitehead and Worthington, 1982) or (2) a shallow reference level (the boundary between AAIW and upper NADW, roughly 1200 db or $\theta \approx 4.7°C$; Wust, 1955; Molinari *et al.,* 1992; McCartney, 1993). However, any choice of a uniform isobaric reference level for this section leads to unsatisfactory results in the deep and bottom waters, as illustrated in Figure 3. Here we show net transports of AABW and NADW across 11N as a function of reference level, after balancing the 13.6 Sv of Ekman and shallow NBC transports by the addition of a small barotropic velocity (v_o) to the section. (Note that in most previous studies there have been no integral constraints on net mass transport, either because they were regionally limited or because insufficient data existed to determine other contributions.) The maximum northward AABW transport that can be obtained is 0.4 Sv, much lower than documented values of 2 to 4 Sv in the tropics (Wright, 1969, 1970; McCartney and Curry, 1993); moreover, maximum southward transport of NADW, expected to be on the order of at least 10 Sv, is only 4 to 5.5 Sv if AABW transport is to be northward. (If an isothermal reference level is used in place of an isobaric one, it is actually impossible to obtain simultaneously both southward-flowing NADW and northward-flowing AABW. Unless otherwise specified all reference levels in the remainder of this paper will be isobaric.) We could allow the reference level to vary continuously across the section, but instead we have chosen a pared down minimalist approach to gain insight into the robust large scale circulation features.

Specifically, we have chosen to subdivide the section into four regions (Fig. 2), which appears to be the minimum number that can represent the different flow regimes adequately at this location. From west to east, the four divisions are defined as Regions 1, 2, 3, and 4. Since the MAR presents a barrier to cross-basin communication of waters colder than about 2.4°C, we separate the western and eastern basins at station 52. Due to the paucity of previous data east of the MAR, we find no compelling basis *a priori* for varying the reference level across this part of the transect. However, in recent decades extensive measurement programs within the western basin of the tropical North Atlantic indicate important zonal structure in the meridional circulation (Molinari *et al.,* 1992; McCartney, 1993), suggesting further subdivision of this basin as indicated in Figure 2. These waters move generally southeastward in the western half of this basin and northwestward in the eastern half, as suggested by isopycnals sloping upward toward the MAR. To allow for this gyre, we choose the boundary between Regions 2 and 3 at station 59, where the dogleg to the southwest begins. This choice is based largely on observations indicating that in the tropical North Atlantic the DWBC extends roughly 800 km offshore of the western shelf break (Molinari *et al.,* 1992). Furthermore, within the deep waters of the 11N transect, the highest values of dissolved oxygen and the lowest values of silicate (indicative of NADW) lie primarily in the westernmost 1000 km (Fig. 2d,e). Finally, within the southward flowing waters of the DWBC itself, the core of upper NADW is found inshore of the core of lower NADW. The division between Regions 1 and 2 is located 175 km offshore of the shelf break near 50W, where observations by Molinari *et al.* (1992) indicate the boundary occurs between the inshore, upper NADW core and the offshore core of lower NADW. We emphasize that these distinct boundaries are a matter of convenience, and that they are expected only to anticipate the gross horizontal structure of meridional circulation in the western basin.

To provide guidance in selecting reference levels for each region, we have plotted the transport per unit depth relative to the bottom for each region, as well as for the section as a whole. In Region 1 (Fig. 4b) we see the well-defined core of northward shear in the AAIW, centered at about 800 m, with the expected southward core of upper NADW just beneath it. In the long term, we expect these two water masses to be flowing in opposite directions, but strong time variability in this area, primarily due to deep-reaching eddies such as those found in current meter records by Johns *et al.* (1990), might introduce doubt as to whether that was the case at the actual time the data were acquired. However, the 800 m floats of Richardson and Schmitz (1993) indicated that AAIW at the western boundary flowed generally northward from January–June, 1989, while nearly all floats at the 1800 m level indicate consistently southward flow; hence in Region 1 we choose a reference level between these two water masses, at 1100 db.

Choosing reference levels in Regions 2 and 3 is somewhat more difficult since in

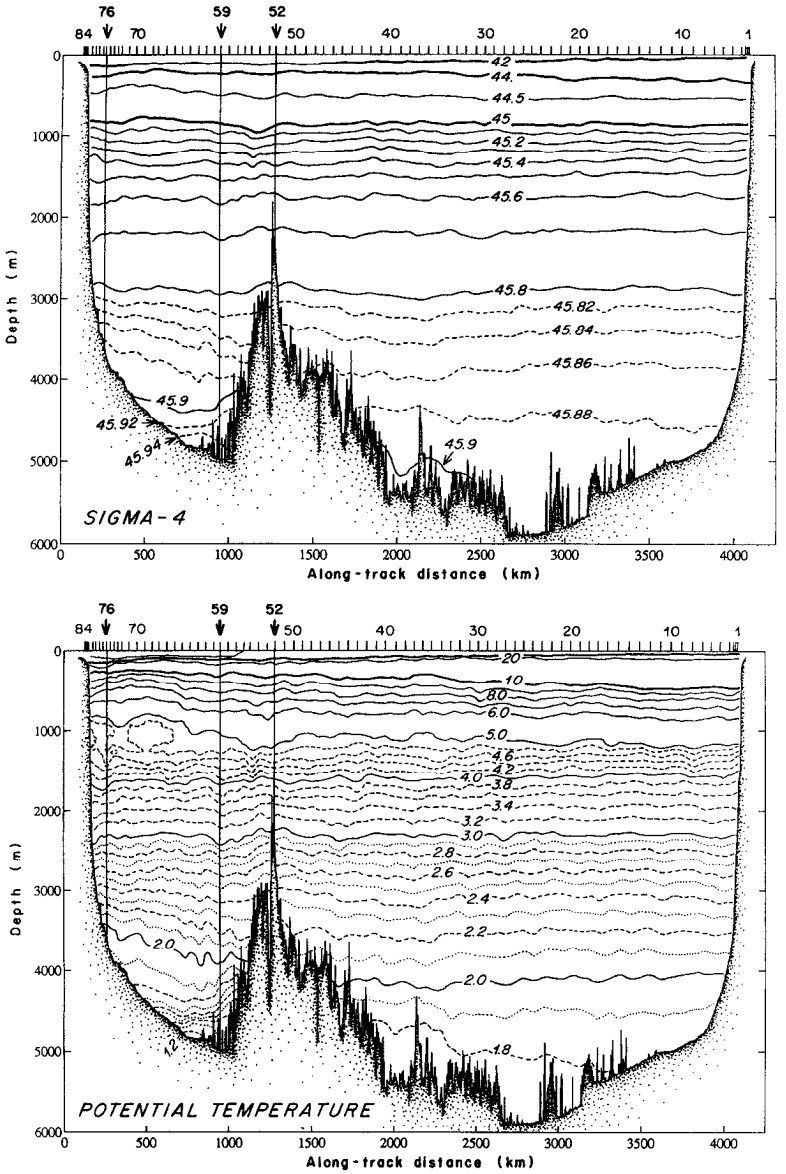

Figure 2. Property distributions along the 11N section from French Guiana (on the left) to Senegal, as a function of depth (m) and along track distance (km): (a) σ_4, (gm/cm^3), (b) potential temperature (°C), (c) salinity (ppt), (d) dissolved oxygen (ml/l), and (e) silicate (μmol/l).

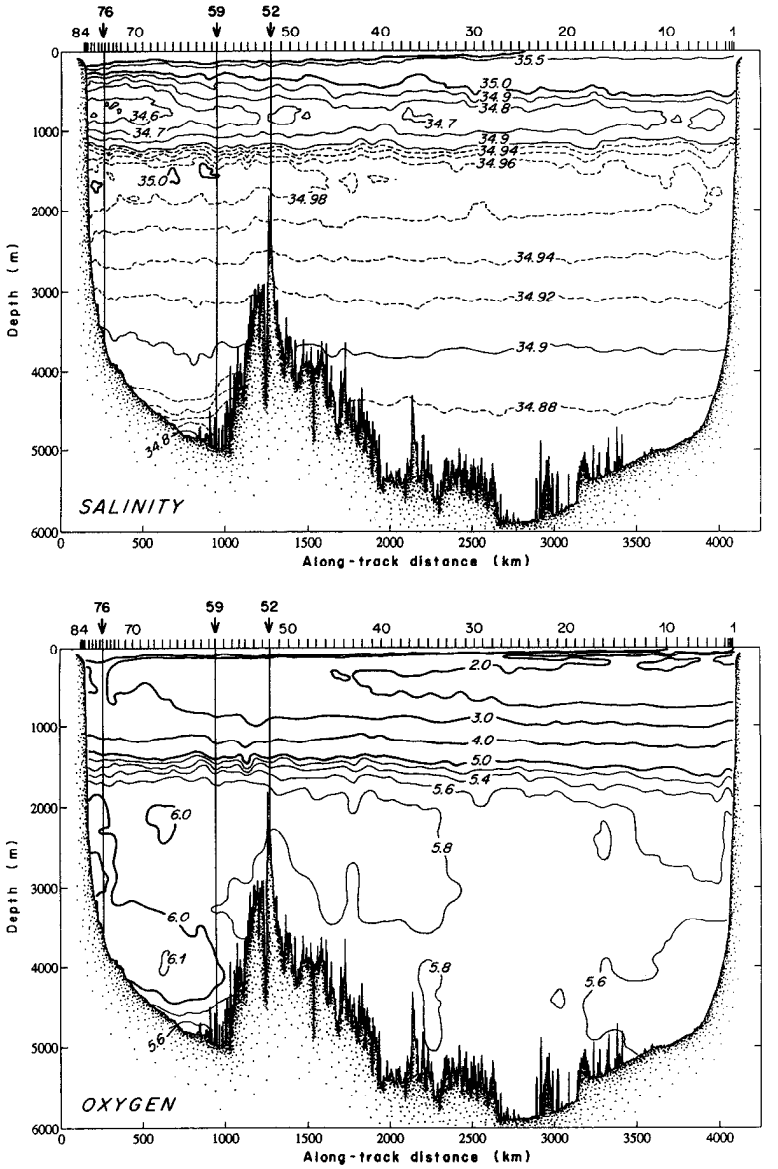

Figure 2. (Continued)

contrast to Region 1, the shear in these regions is essentially single-signed throughout the bottom and deep waters. Furthermore, the shear is of opposite sign in Region 2 as compared to Region 3. Unfortunately, the few floats deployed across these much broader regions are of little help in determining our reference level, for they were

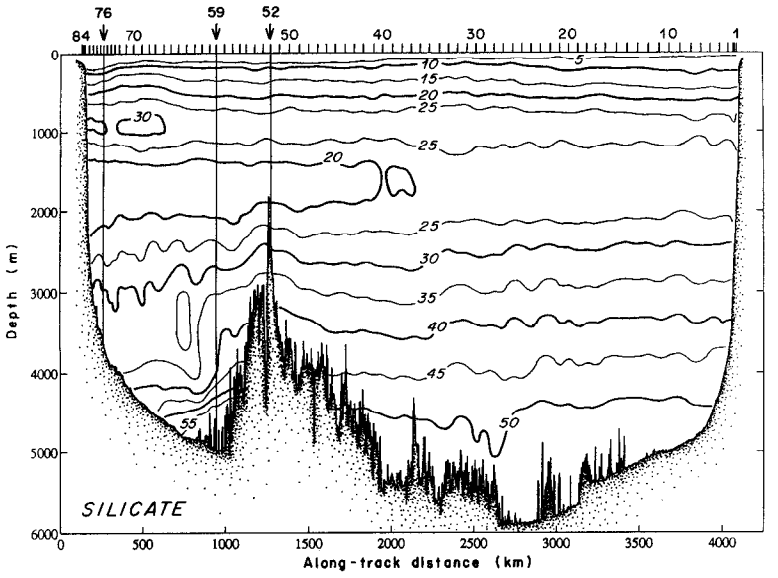

Figure 2. (Continued)

subject to extremely strong time and space variability. Choosing a deep reference level (between NADW and AABW) in these regions would yield circulation patterns inconsistent with nearby observational evidence for the deep cyclonic recirculation gyre as well as with the distribution of tracers in this section. For example, the strong dissolved oxygen maximum in the western half of the basin (Fig. 3d) must have its origin in the northern North Atlantic and is representative of the strong southward

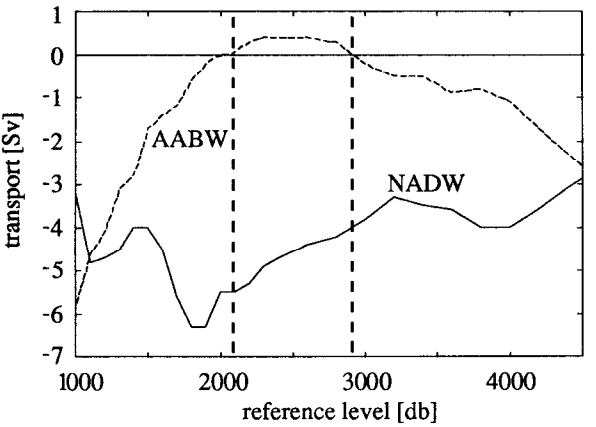

Figure 3. Transports of AABW and NADW, as defined in Table 1, as a function of reference level for the entire 11N section. If a reference level is chosen such that AABW is constrained to go northward (i.e., between the dashed lines shown above), the resulting NADW transport is between −4 and −5.5 Sv.

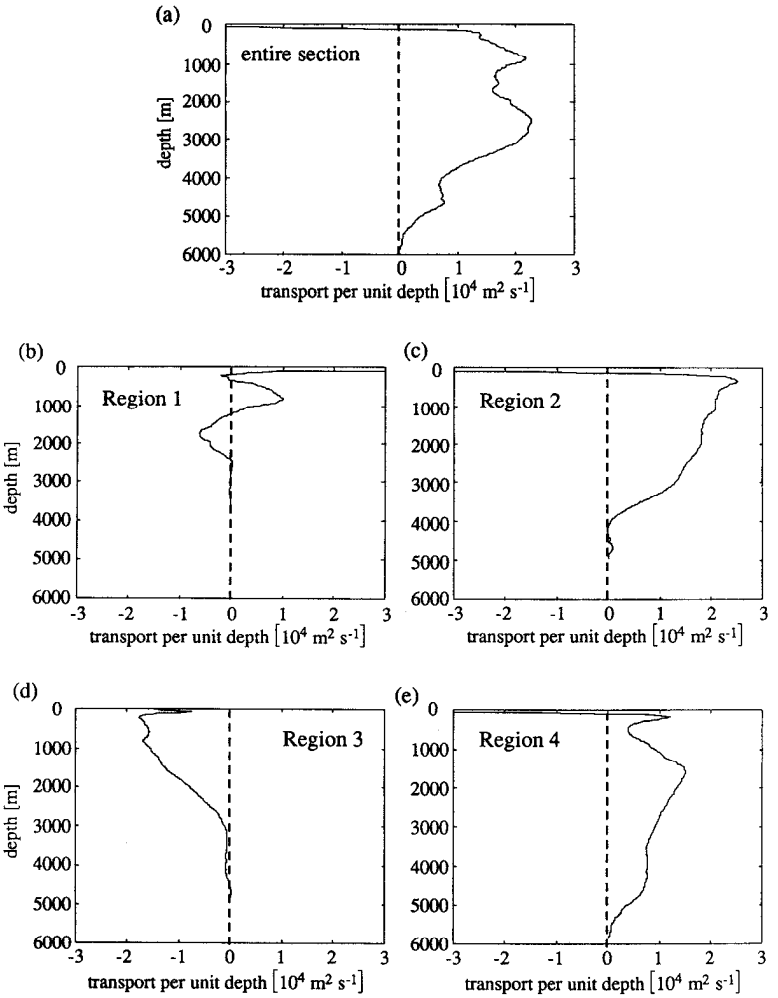

Figure 4. Transport per unit depth relative to the bottom, for (a) the entire section, (b) Region 1, (c) Region 2, (d) Region 3, and (e) Region 4.

flowing DWBC. If we choose a reference level in Region 2 below 3000 m, we would find the magnitude of the DWBC to be less than 15 Sv—much smaller than most recent DWBC transport estimates of between 20 and 45 Sv (Speer and McCartney, 1991; Molinari *et al.,* 1992; Johns *et al.,* 1993; McCartney, 1993).

Thus we now consider the set of all possible reference level combinations (in 100 db increments) between 1000 and 3000 db for Region 2, and 1000 and 4000 db for Region 3. Figure 5 shows contours of AABW transport (5a) and NADW transport (5b) in the western basin for this parameter range. First we constrain our reference level choice by demanding net AABW transport to be greater than −0.5 Sv, i.e. at

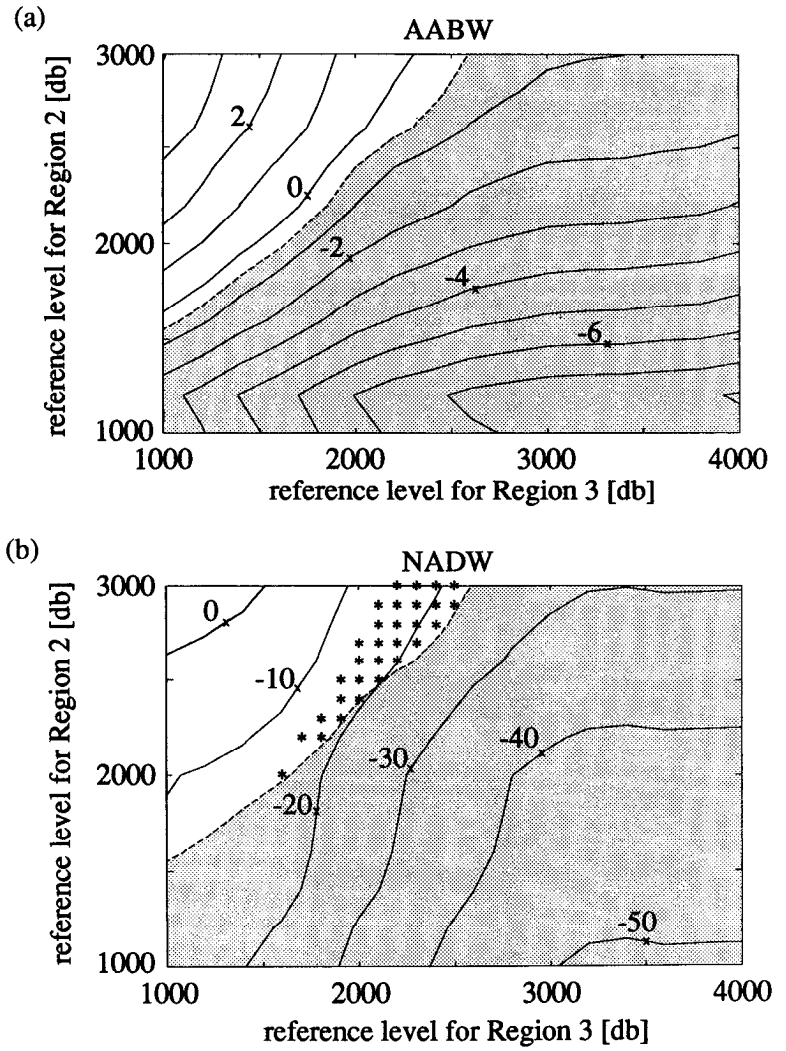

Figure 5. Contour plots of the western basin transports of (a) AABW and (b) NADW as a function of the reference levels in Regions 2 and 3. The reference level in Region 1 is held constant at 1100 db. (Mass is not balanced since reference levels for Region 4 have not yet been chosen.) The shaded areas represent the combinations of reference levels which give unrealistically large southward AABW transports within the western basin, while the asterisks in (b) are the thirty reference level combinations chosen such that AABW transport is greater than −0.5 Sv, and southward NADW transport is maximized.

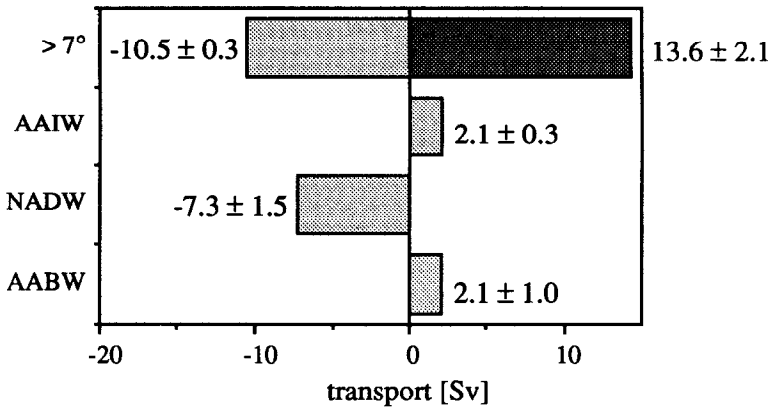

Figure 6. Lightly shaded bars illustrate the mean geostrophic transports in four temperature classes for the 30 reference level combinations depicted in Figure 5b, while the darkly shaded bar represents the sum of the Ekman and shallow NBC transport components. Error bars include the uncertainties in the bottom triangle, Ekman, and shallow NBC transports.

most 0.5 Sv southward. The shaded region in Figure 5 (including 524 out of the 651 possible combinations) is thus eliminated. This constraint is moderate, since McCartney and Curry (1993) predict a northward cross-equatorial flow of 4.3 Sv. Because we have observed that net southward transport of NADW is small for uniform reference levels, we also choose to maximize southward NADW transport in the western basin. (Note that after mass is balanced by uniformly adding a typical positive v_o to the section, the southward flowing western basin NADW transport will decrease in magnitude by roughly 3 Sv.) The asterisks on Figure 5b represent the 30 choices that satisfy these conditions.

Eastern basin reference levels are now chosen such that total NADW transport (across the entire section) is maximized for each of these 30 combinations. After examining eastern basin reference levels between 1000 and 5000 db, we find that for every one of the 30 combinations found above, total NADW transport is maximized for a choice of 2100 db.

In summary, levels of no motion have been chosen that give acceptable western basin AABW transport and simultaneously maximize total NADW transport. These criteria yield reference levels of 1100 db for Region 1, 2100 db for Region 4 and a range of possible reference level combinations for Regions 2 and 3, as depicted in Figure 5b. Where bottom depths are shallower than the reference level, velocities are referred to the deepest common level of the station pair. (Additional details of the mechanics of the geostrophic calculation, including a description of the weighted shear bottom triangle method used in this analysis, can be found in Friedrichs (1993).) The resulting net transports are shown in Figure 6. Error bars include the uncertainties in the bottom triangle, Ekman, and shallow NBC transports. The error

due to reference level choice is assumed to be equal to the standard deviation of the thirty different reference level calculations, and in this case is insignificant in comparison to the other sources of error.

The transport results shown in Figure 6 show marked improvement over the initial results for uniform reference levels discussed above. For instance, the net transport of AABW is now northward, in agreement with previous current meter, tracer and CTD data. The southward transport of NADW has doubled, but is still considerably smaller than that obtained in previous mid-latitude studies of IGY data (Hall and Bryden, 1982; Roemmich and Wunsch, 1985). Further discussion of the discrepancy in these results is postponed to Section 4. In the following section we first examine in detail the circulation patterns resulting from the data analysis methods described above, and compare these with other results of recent float, current meter and CTD studies.

3. Horizontal circulation

Volume transport in eight temperature classes (Table 1) is computed for each of the 30 allowed reference level combinations. Net transports for each layer in the four different regions are shown in Figures 7(a–d), where the error bars include the uncertainties in the bottom triangle, Ekman, and shallow NBC transports, as well as the error in reference level choice (again assumed to be the standard deviation of the thirty estimates). In contrast to the net transport calculations (Fig. 6), reference level errors dominate the error bars of Figures 7(a–d). The bottom triangle errors are significant only in the AABW transports, and the uncertainties in the Ekman and shallow NBC transports only introduce important errors in the eastern basin. Additional details of the horizontal structure are highlighted by Figure 8, where transport integrated eastward from the western boundary is shown for each layer. Before beginning a detailed description of the deep and bottom water circulation, a brief overview of the shallow water circulation will be presented.

a. Shallow waters. $\theta > 4.7$°C. Integrated transports of the surface and thermocline waters are shown in Figures 8(a–c). The NBC is evident in the upper two layers as a strong northwestward flowing current banked up against the western boundary and extending roughly 250 km offshore, attaining a transport of 11.8 Sv (9.3 Sv of $\theta > 24$°C water and 2.5 Sv of $12° < \theta < 24$°C water). A number of recent investigations have focused on the NBC (Philander and Pacanowski, 1986a, b; Johns *et al.,* 1990; Candela *et al.,* 1992; Johns *et al.,* 1992) and have shown that this strongly seasonal current may range from roughly 10 Sv in the spring to as much as 30–35 Sv in the fall. Our estimate of 11.8 Sv agrees well with previous March observations of 10–15 Sv (Candela *et al.,* 1992; Johns *et al.,* 1992).

Farther offshore of this current, a large southeastward counterflow exists throughout the surface and thermocline layers, with a net magnitude of 25.4 Sv southward

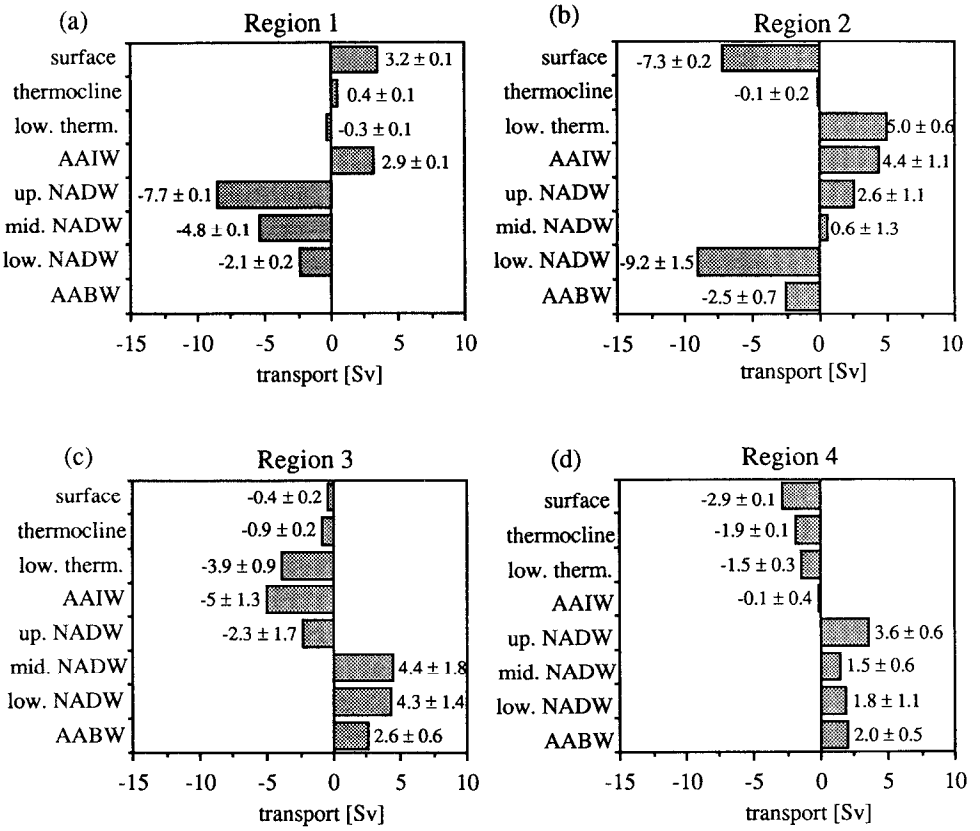

Figure 7. Geostrophic transport in eight temperature classes (Table 1) for (a) Region 1, (b) Region 2, (c) Region 3, and (d) Region 4.

(13.5 + 7.8 + 5.1 Sv). Although typically the North Equatorial Countercurrent (NECC) is absent in March (Csanady, 1985; Richardson and Walsh, 1986; Johns *et al.,* 1990), a recent study by Katz (1993) shows that in March 1989 it was present with an uncommonly large transport of 14 Sv. Thus a portion of this counterflow may be the NECC, or a retroflection eddy that has been pinched off from the NBC retroflection, or perhaps some combination of both. The remainder of the western basin is dominated by eddy activity in all three layers, with net northward flows on the order of 5 Sv in each. The eastern basin is also characterized by eddy activity, with barely significant net transports in layers 2 and 3 ($7° < \theta < 24°C$). Since the 24°C isotherm outcrops roughly 2800 km from the west coast, Figure 8a shows no additional transport in the easternmost 1200 km.

Table 2 compares our results with those of a recent study by Schmitz and Richardson (1991), who examined the origin of the surface and thermocline waters within the Florida Current. For each temperature class, they determined how much

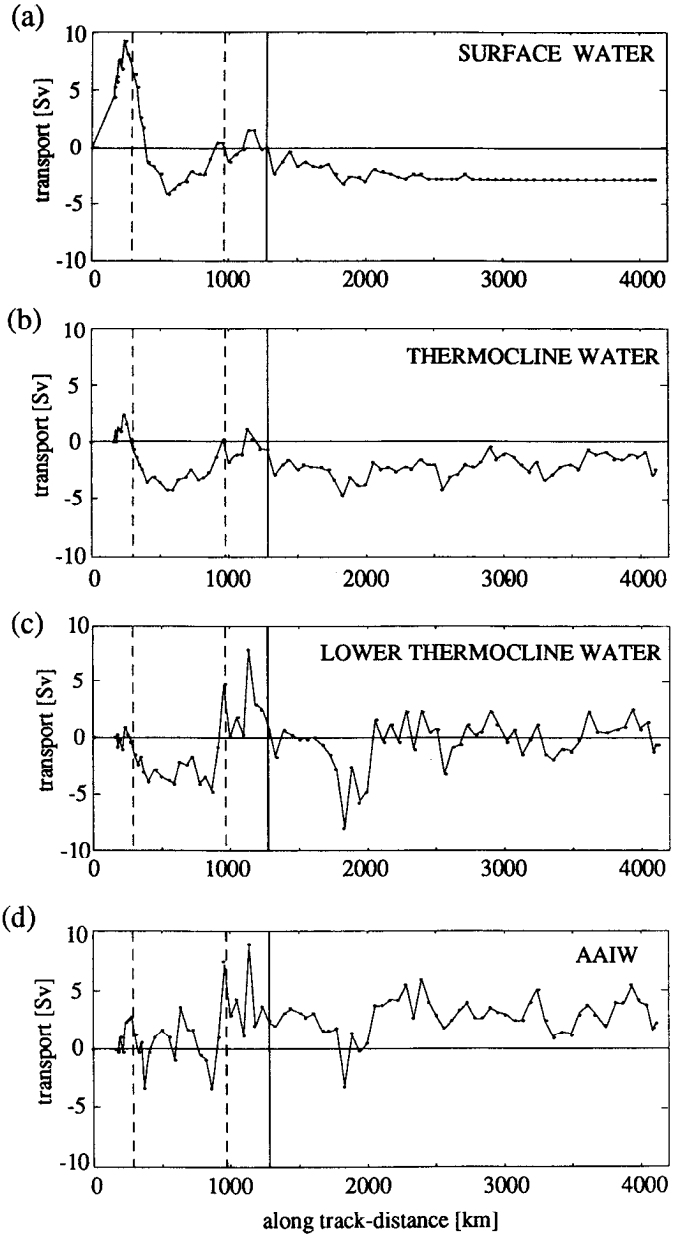

Figure 8. Northward transport integrated seaward from the western boundary, as a function of along-track distance for: (a) surface water, including the absolute shallow NBC transport, but not the Ekman transport over the remainder of the section, (b) thermocline water, (c) lower thermocline water, (d) AAIW, (e) upper NADW, (f) middle NADW, (g) lower NADW, and (h) AABW. The solid vertical line represents the center of the MAR, while the dashed lines indicate the divisions between Regions 1, 2 and 3.

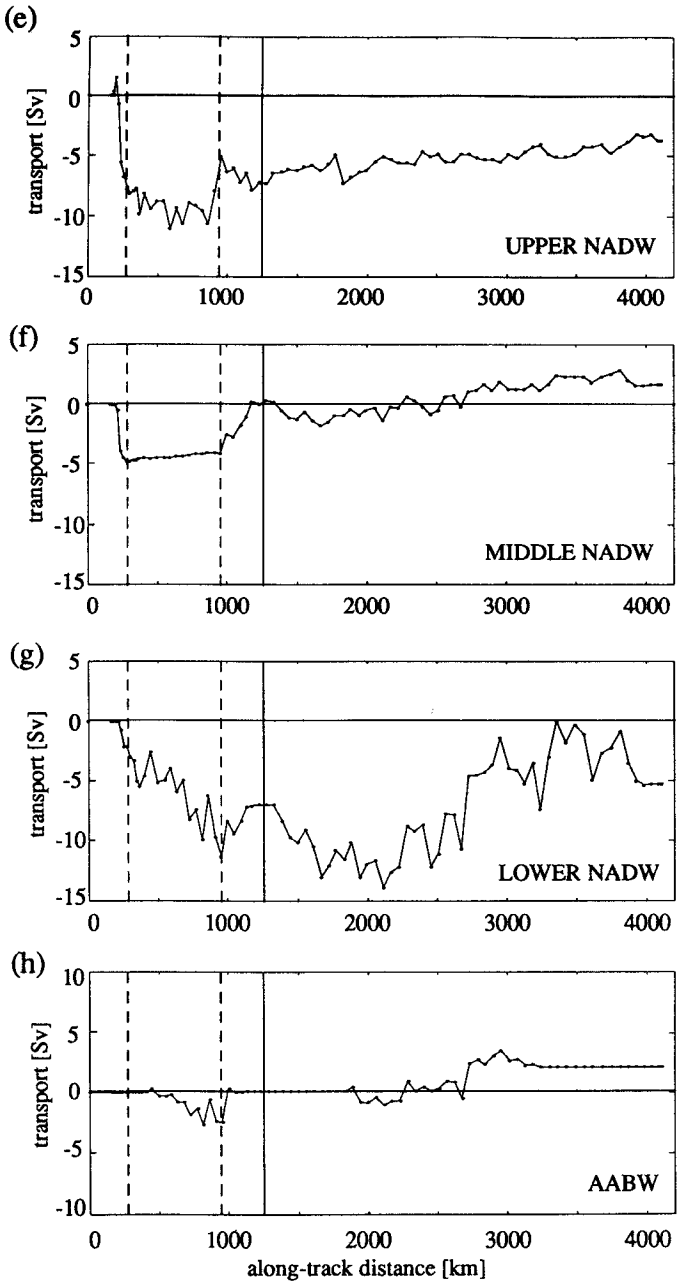

Figure 8. (Continued)

Table 2. Transport in three temperature classes through the Florida Straits and across 11N. The Florida Straits values are denoted as the sum of water of South Atlantic (SA) and North Atlantic (NA) origin according to Schmitz and Richardson (1991). Transports crossing 11N are given for the entire section, and for the western thousand kilometers (i.e. Regions 1 and 2). All transports are in Sverdrups.

	Schmitz and Richardson (1991)	11N: Entire section	11N: West 1000 km
$\theta > 24°C$	7.1 + 1.8 (SA) (NA)	10.5 ± 1.1	5.4 ± 1.1
$12° < \theta \leq 24°C$	0.8 + 13.0 (SA) (NA)	−2.7 ± 0.5	0.2 ± 0.2
$7° < \theta \leq 12°C$	5.0 + 1.1 (SA) (NA)	−1.0 ± 1.7	4.7 ± 0.6

of the transport was of North Atlantic versus South Atlantic origin. For the 11N section we tabulate transports for the same classes (where the shallow NBC and climatological (March) Ekman transports have been included in the surface water) across the entire section as well as transports in the westernmost 1000 km alone (i.e. Regions 1 and 2), since these would be more likely to feed the Florida Current. In each of the three layers, the amount of Florida Current transport of South Atlantic origin (Schmitz and Richardson, 1991) compares well with the northward transport of the same layers across the western 1000 km of this section.

We now consider the circulation and transports of AAIW, about which very little is known (Schmitz and McCartney, 1993). The strong eddy activity characterizing this water mass causes the AAIW transports to be extremely sensitive to the horizontal limits of integration. In Figure 7, for example, the transports of AAIW which indicate an anticyclonic circulation within the western basin are primarily an artifact of the specific divisions we have chosen between Regions 1–3. This is evident from Figure 8d, which shows little evidence of such a well-defined anticyclonic flow pattern. Within the eastern basin Figure 8d indicates considerable eddy activity with only small net transports of AAIW. This is consistent with the salinities found at 800 m in the eastern basin, which are slightly higher than those found at similar depths within the western basin (see Fig. 2c).

One of the few studies that yield AAIW transport estimates with which these results can be compared is that of Richardson and Schmitz (1993). They present results for neutrally buoyant SOFAR floats deployed at nominal depths of 800 m along the cruise track of the 11N section. Within roughly 450 km of the western boundary, the floats were dominated by a northwestward along-boundary transport. The transport per unit depth of these floats, when integrated from the western boundary to roughly 450 km offshore, reached a maximum of $5.8 \pm 1.8 \times 10^3$ m^2 s^{-1}. A similar integration of our CTD data at depths between 700 and 900 m yields a

maximum transport per unit depth of roughly 7×10^3 m^2 s^{-1}, in good agreement with the value of Richardson and Schmitz (1993).

b. Deep waters. $\theta < 4.7$°C. In comparison with the AAIW, the NADW is a rather well studied water mass. As early as in the 1930's (Wust, 1935) the NADW was found to have three cores, each with its own distinct characteristics and formation site. Wust identified the upper NADW by a deep salinity maximum and attributed this to the Mediterranean outflow. He also found the middle NADW to contain a maximum in dissolved oxygen concentration which he traced back to the Labrador Sea. He believed that the lower NADW, characterized by a second, deeper oxygen maximum, was formed by deep winter convection in the region south of Greenland. More recent studies have supported the existence of the three NADW cores, which are most clearly identified by means of the chloroflourocarbon F11 (Molinari *et al.,* 1992). The upper NADW is characterized by a maximum in F11, below which lies a relative minimum of F11 associated with the middle NADW. A second F11 maximum identifies the lower NADW. Before launching into individual discussions of each of these three NADW layers, we first begin with a look at the DWBC, the most frequently studied feature of the deep North Atlantic circulation.

Definitions of the DWBC vary widely, depending primarily on the type of data (CTD's, current meters, or floats) used to obtain estimates of its transport. In this study the magnitude of the DWBC is defined as the maximum southward transport of waters with $\theta < 4.7$°C integrated seaward from the western boundary. As shown in Figure 9, this definition yields a transport of 26.5 ± 1.8 Sv for the DWBC, where the error bar includes the uncertainties in the bottom triangle transport, as well as the reference level error. (As a result of the small percentage of the total section area the DWBC occupies, the uncertainties in the Ekman and shallow NBC transports are insignificant.) Previous DWBC transport estimates (Table 3) range from as low as 7 Sv (Swallow and Worthington, 1961) to as high as 35–45 Sv (Leaman and Harris, 1990; McCartney, 1993), with most in the range of 20–30 Sv.

Molinari *et al.* (1992) have speculated that within the tropical North Atlantic a large portion of this DWBC transport may be recirculated, as it has been suggested to do farther north in the mid-latitudes (Leaman and Harris, 1990; Lee *et al.,* 1990), while McCartney (1993) has also postulated that as much as two-thirds of the DWBC may be recirculating back northward. These conclusions have been reached primarily on the basis of property distributions within the DWBC and across the basin. (The term "recirculation" is used to convey that adjacent southward and northward flows are not of distinct northern and southern origin but are linked to one another to the north and south.) Results from the present analysis confirm the existence of at least a partial recirculation of the DWBC waters, and furthermore yield an estimate of 13.3 Sv for the northward flow of deep water over the western flank of the MAR (Fig. 9). These recirculations are described in more detail below.

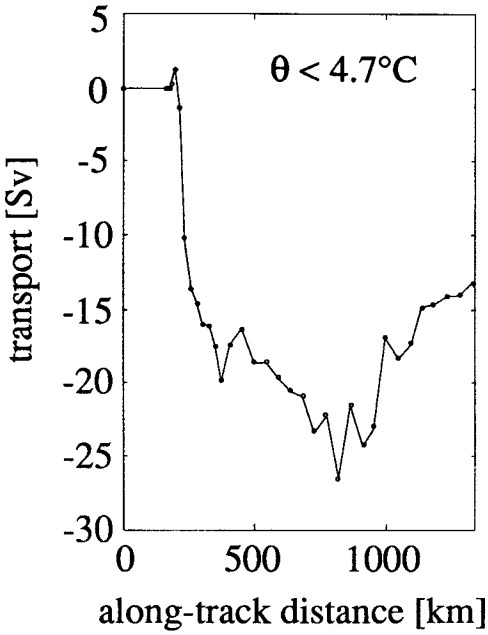

Figure 9. Transport of θ > 4.7°C integrated seaward from the western boundary. The magnitude of the DWBC, as defined in text, is 26.5 Sv. Roughly half of this returns northward over the western flank of the MAR.

Each of the three NADW layers, as well as the AABW, will now be discussed individually. In addition to the integrated transport of Figures 8(e–h), we have also included schematic cartoons of the circulation patterns for each of these water masses (Fig. 10a–d). These cartoons are based on the results of this study as well as evidence provided by previous tropical Atlantic studies (specific studies will be cited in the following paragraphs); however, the transport values shown on Figure 10 are exclusively from this study, and are thus meant to quantify transports across the 11N section.

In Figure 8e we see the strong southward flow of upper NADW banked up against the western boundary achieving a maximum southward transport of 10–12 Sv. Within Region 2 a very narrow northward current is located directly over the deepest part of the western basin. We are confident that this offshore flow represents a recirculation of the upper component of the DWBC, since the properties generally associated with this water mass are evenly distributed throughout these regions. The salinity >35.0 contours and the oxygen >6.0 contours appear only in these two regions, and are absent from Regions 3 and 4. Although the upper component of the DWBC has a magnitude of nearly 12 Sv, this northward recirculation reduces this layer's net (western basin) southward flow to 6 Sv. According to Richardson and Schmitz's (1993) SOFAR float trajectories, this current sometimes continues southward across

Table 3. Estimates of the DWBC within the tropical North Atlantic.

	Latitude	DWBC [Sv]
Stommel and Arons, 1960*	35N	20
Swallow and Worthington, 1961†	33N	7
Barrett, 1965†	35N	12
Amos *et al.*, 1971*	30N	22
Richardson, 1977†	35N	24
Lai, 1984‡	28N	24
Fine & Molinari, 1988*	26.5N	24
	19N	8
Lee *et al.*, 1990‡	26.5N	33
Leaman and Harris, 1990†	26.5N	35
Speer and McCartney, 1991*	10N	25
Molinari *et al.*, 1992*	4–14.5N	26
McCartney, 1993*	52W	35–45
Johns *et al.*, 1993‡	8N	22
this study*	8N	27

*geostrophy.
†geostrophy with direct current measurements.
‡direct current measurements.

the equator, while at other times it veers eastward along the equator. These features are shown schematically in Figure 10a. (Note that the locations of the northern and southern closures of the western basin recirculation gyre are only meant to represent possible closure sites based on previous studies and surrounding topography; clearly the sites of the gyre closures cannot be ascertained by the 11N section alone.) Region 3 is characterized by a small southward flow of roughly 2 Sv over the western flank of the MAR. This flow may continue southward and become entrained into the eastward flow along the equator and/or the southward flow along the western boundary, or it could flow eastward (over the MAR) and perhaps interact with the weak northward transport that is found evenly distributed over the eastern basin. We have not tried to depict the latter flow in Figure 10a, as it could occur at any location and be quite diffuse.

We can make quantitative comparisons with a number of recent studies that have concentrated on deep water transport within the western basin. For instance, after analyzing a number of hydrographic sections between 0 and 14.5N taken between 1987 and 1989, Molinari *et al.* (1992) arrived at a smaller average value of -4.4 ± 2.3 Sv for the transport of upper NADW within the DWBC. Speer and McCartney (1991) also determined upper NADW transport from hydrographic data in the tropical Atlantic, and found a transport of $(-16.8, -12.6)$ Sv across (13N, 7–10N) near the western boundary between 1200 and 2900 m depths. For comparison, using this alternate definition we find a transport of -11 Sv, in close agreement with their

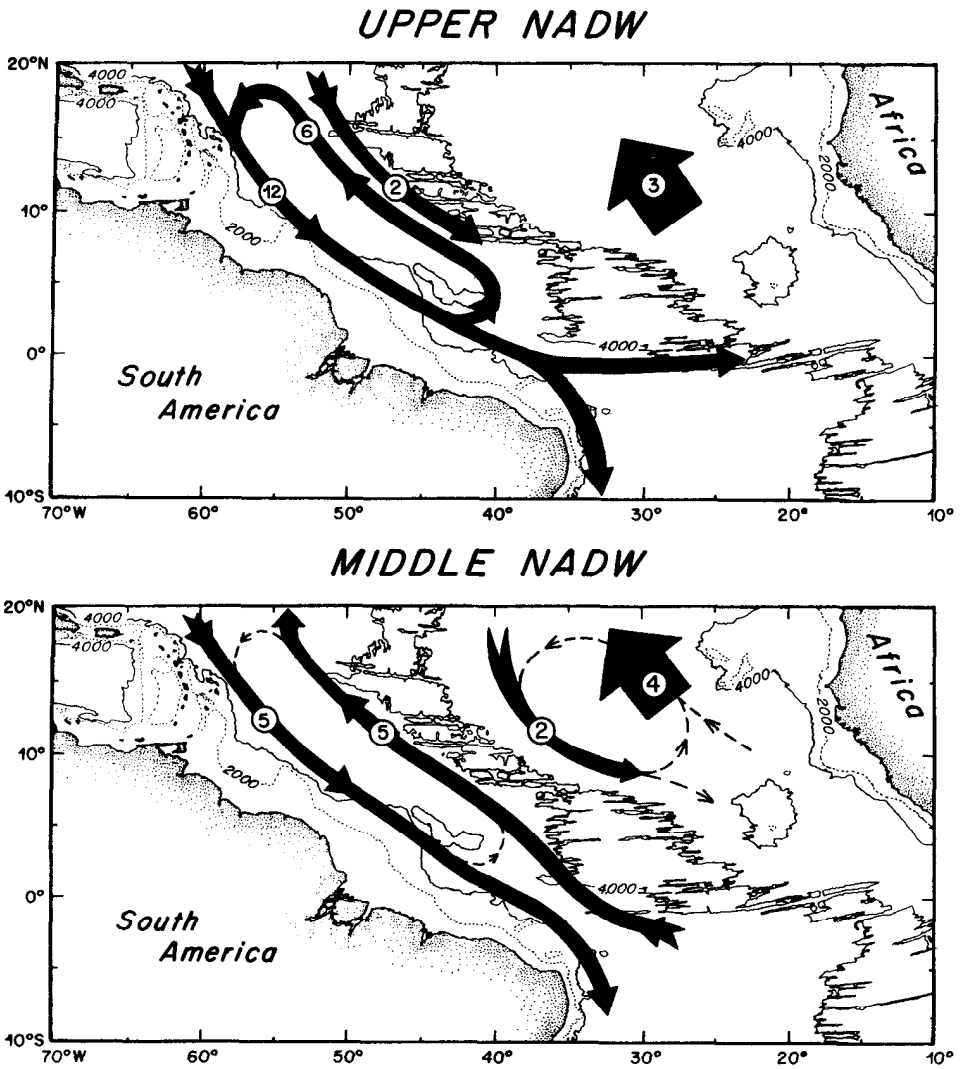

Figure 10. Schematic circulation patterns in the tropical Atlantic, for: (a) upper NADW, (b) middle NADW, (c) lower NADW, and (d) AABW. Transports and circulation patterns crossing 11N are direct results of this study, whereas the arrows extending away from the 11N section are based on a synthesis of existing information on the tropical Atlantic circulation (see text.)

more southern estimate (recall that at the western boundary, the "11N" section terminates at about 5N). Finally, the SOFAR float data of Richardson and Schmitz (1993) also give supporting evidence for a strong southward flow of upper NADW along the western boundary. Integrating the velocities obtained from their 1800 m floats over the 100 km width of the current, they found a transport per unit depth of

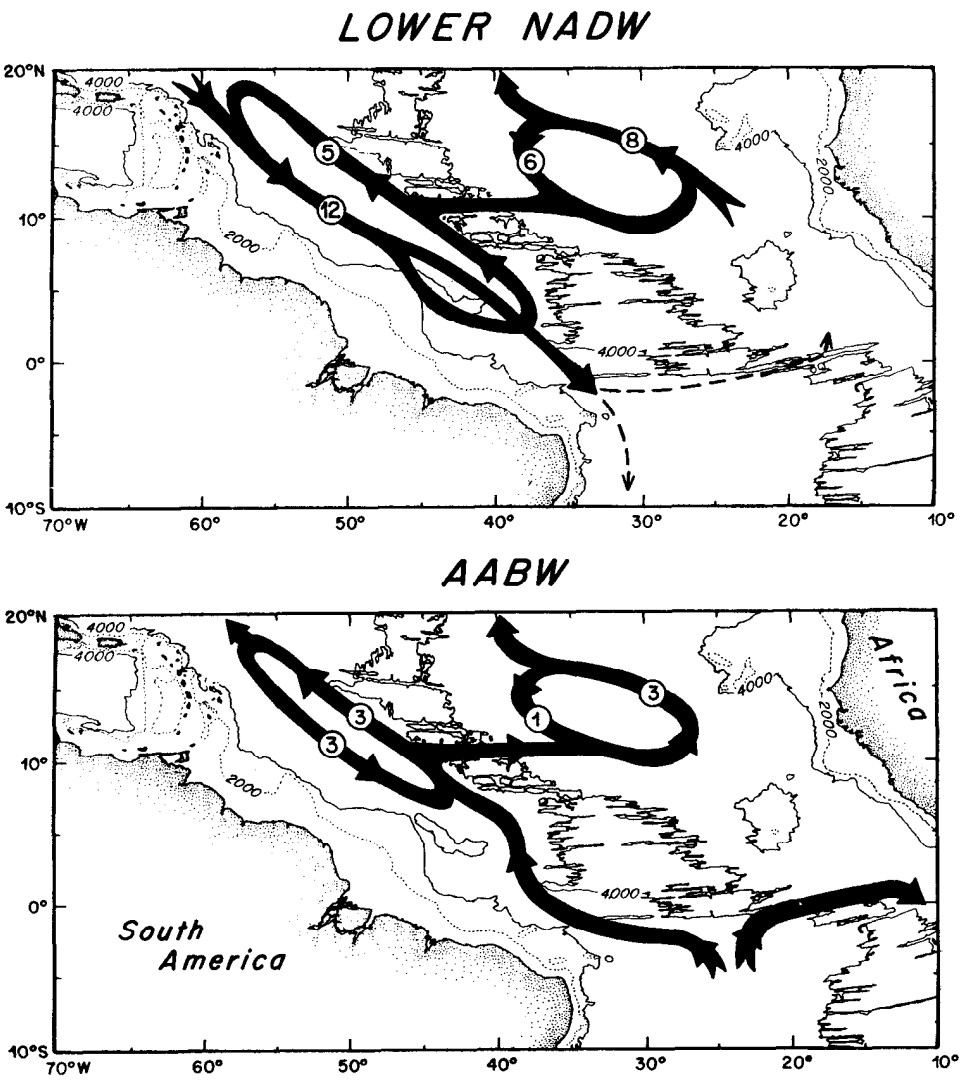

Figure 10. (Continued)

-13.8×10^3 m^2 s^{-1}. A similar 100 km zonal integration of our CTD data between 1700 and 1900 m yields an average transport per unit depth of -10.5×10^3 m^2 s^{-1}, in good agreement with the value obtained by Richardson and Schmitz. However, total upper NADW transport reported by them (-15 Sv) differs from our analogous value (-8 Sv) because they chose different vertical limits of integration. While they assume this water mass extends from 900–2800 m, our CTD data show that it extends only between 1500 m and 2500 m. (This can be seen by the vertical extent of the silicate minimum and the salinity maximum at the western boundary, as shown in

Figures 3c,e.) Richardson and Schmitz also estimated an upper NADW recirculation of 5.8 Sv, closely matching the 6 Sv of recirculation found in this study (Figs. 8e, 10a). As a result of the large possible errors Richardson and Schmitz associated with their value, this agreement may be fortuitous.

The middle core of NADW (Figs. 8f, 10b) also contains a strong southward flow banked up against the western boundary. The transport of this flow, located directly beneath the core of upper NADW, is −5 Sv and agrees well with the -6.3 ± 2.1 Sv of middle NADW transport observed by Molinari *et al.* (1992). Within the center of the western basin there is almost no net flow or eddy activity, while a strong northward current is located over the western flank of the MAR. The origin of this current is not well known. The oxygen values in this flow are about 0.2 ml l^{-1} lower than those in the middle NADW of the DWBC, suggesting that this water mass may be coming from the South Atlantic and hence is not dominated by recirculating boundary current waters. It is possible, for example, that some of the northward flowing deep water observed in the eastern South Atlantic (Warren and Speer, 1991) flows into the western basin via one or more of the various fracture zones in the MAR and continues northward along the western side of the MAR. On the other hand, although the quiet interior of the western basin middle NADW suggests little interaction between these two branches of flow, we cannot rule out the possibility that some part of this water recirculates along with the layers of NADW above and below it; this possibility has been illustrated by dashed lines in Figure 10b. In either case, since the magnitudes of these two opposing western basin currents are equal and opposite, the net flow of middle NADW within the western basin is indistinguishable from zero.

Within the eastern basin, Figure 8f shows a small southward flowing current of middle NADW banked up on the eastern flank of the MAR, and a slightly larger net northward flow evenly distributed over the remainder of the section. This is presented schematically in Figure 10b. The wide northward-flowing current may be directly linked to the middle NADW found by Warren and Speer (1991) flowing northward across 11S, while the narrow southward-flowing current may either flow directly across the equator, or participate in a recirculation of unknown extent. The lower oxygen values hugging both flanks of the MAR at these levels (Fig. 2d) suggests some link to the northward current in the western basin as well; but because numerous locations along the MAR would permit such a flow, we have not tried to depict this connection in Figure 10b. Unfortunately, there are few previous transport estimates with which these proposed circulation patterns can be compared, since most previous deep circulation studies have been carried out within the western basin, and furthermore since the NADW frequently has been divided into only two layers.

The integrated transport of lower deep water is shown in Figure 8g, while schematic circulation patterns are illustrated in Figure 10c. Within the western basin

we see that the DWBC in this layer is noisier and less western intensified than in the upper and middle NADW cores. The southward transport of lower NADW is also located significantly offshore of these two shallower cores, resides primarily within Region 2, and in Figure 10c is shown to split at 5N and flow around both sides of the Ceara Rise (Schott *et al.,* 1993). The transport of this core of the DWBC is found to be −12 Sv and agrees well with the results of Molinari *et al.* (1992) who found an average lower NADW transport of -13.0 ± 2.7 Sv for sections between 0 and 14.5N. In a recent study by Speer and McCartney (1991), the lower NADW, defined as all flow between 2900 and 4400 m, was found to transport −8.4 Sv along the western boundary across 13N and −13.2 Sv across 52W between 7 and 10N. Applying this definition to our data, we find an intermediate value of −10.5 Sv flowing across our section.

Roughly 5 Sv of the lower NADW is found flowing northward along the western flank of the MAR, directly beneath the middle NADW. This appears to represent at least a partial recirculation of the lower NADW from the boundary current, since the deepest water in this layer has relatively uniform properties across Regions 2 and 3; e.g. the 6.0 ml l^{-1} oxygen contour of Figure 2d extends well into Region 3. Although the latitudinal extent of this recirculation is not yet well established, Figure 10c shows this cyclonic gyre extending nearly to the equator (McCartney, 1993), and perhaps as far north as 15–25N (Molinari *et al.,* 1992; McCartney, 1993). The shallower portion of this layer is both somewhat fresher (Fig. 2c) and characterized by slightly lower oxygen values (Fig. 2d), which may reflect mixing with the overlying northward middle NADW current described above. It is also possible that the lower oxygen values of this northward flow are enhanced by mixing with low oxygen lower NADW from the eastern basin (Fig. 2d) which may be entering the western basin via the Vema Fracture Zone. (Applying our reference level choices to the Vema stations described by McCartney *et al.* (1991), gives a small $O(1$ Sv) westward transport of lower NADW through the Vema fracture Zone. Since this value may not be significantly larger than its associated error bar, we refrain from putting a directional arrow on the Vema throughflow illustrated in Figure 10c.) Depending of course on the size of this Vema throughflow, we infer that roughly 7 Sv of lower NADW reaches the equator. A small amount of this may continue southward along the western boundary; however it is also possible that this core of the DWBC may proceed eastward along the equator. The fate of this flow is under current investigation with M. McCartney (Friedrichs *et al.,* 1993).

Some degree of lower NADW recirculation is also occurring within the eastern basin; however here the properties are more evenly distributed throughout the basin in the *shallow* portion of the lower NADW. The deepest ($1.8° < \theta < 2.1°$) part of this layer has somewhat lower oxygen in the eastern part of this basin than in the west; this feature is most likely associated with the low oxygen signal found between 3500 and 4400 m at 11S (Warren and Speer, 1991). Within the eastern basin between

2400 and 4000 db, Warren and Speer (1991) found a net 1.8 Sv flowing northward across 11S. Although this pressure interval corresponds roughly to 2.0°–2.7°C and thus contains most of the lower NADW as well as some of the middle NADW, it is reasonable to assume that at least 1 Sv of lower NADW is crossing the equator and flowing into the tropical North Atlantic. Additionally, some of the hypothesized eastward flow of lower NADW along the equator (Friedrichs *et al.,* 1993) may enter the eastern basin via the Romanche Fracture Zone at the equator, and thence be diverted northward, to further contribute to the recirculation gyre illustrated in Figure 10c. The combination of these flows ultimately yields a 2 Sv net northward flow of lower NADW in the eastern basin across 11N.

Beneath the lower NADW resides the AABW. As shown in Figure 6, a net AABW transport of 2.1 Sv is found crossing our 11N section. This result agrees well with the earlier results of Wright (1969, 1970), who found (1.4, 2.7) Sv of AABW crossing (16N, 8N), and those of Whitehead and Worthington (1982) who found 2.0 Sv of AABW crossing 4N; however, these values are slightly smaller than McCartney and Curry's (1993) more recent estimate of 4.3 Sv of cross-equatorial bottom water flow. Transport of AABW integrated seaward from the western boundary is shown in Figure 8h, while a schematic representation of the flow appears in Figure 10d. From these figures we see that this component of the DWBC reaches a magnitude of nearly 3 Sv, agreeing well with Molinari *et al.*'s (1992) estimate (based on sections between 4–14.5N) of 2.2 ± 0.9 Sv, and Johns *et al.*'s (1993) value of 3 Sv from current meter measurements at 8N. Figures 8h and 10d also show a vigorous recirculation of AABW within the western basin associated with a negligible (less than 1 Sv) net northward transport. (We note that this insignificant net flow of AABW in the west is partially an artifact of our definition of AABW; for example, had we defined the AABW to include all water with $\theta < 1.7$°C we would have found a net northward flow within the western basin of 1.1 Sv.) Although at 52W McCartney (1993) finds a much larger 11 Sv AABW recirculation, it is still associated with a very small net western basin AABW transport of only 0.4 Sv.

This small net western basin AABW transport is somewhat counterintuitive, since the Walvis Ridge at 30S blocks northward flow of AABW into the eastern basin of the South Atlantic. However, as shown in Figure 10d, this water may enter the eastern basin of the tropical North Atlantic by means of the Vema Fracture Zone just south of our section. (Additional AABW flows eastward through the Romanche Fracture Zone and is believed to veer southward, since no significant transport of AABW is found flowing through the Kane Gap at 8N, 20W (McCartney *et al.,* 1991).) In fact, given that there is no cross-equatorial flow of AABW within the eastern basin, our result of 2 Sv flowing northward within the eastern basin dovetails nicely with McCartney *et al.*'s (1991) findings of 2.2 Sv flowing eastward through the Vema Fracture Zone. This net northward AABW flow within the eastern basin is associated with a 1 Sv cyclonic recirculation cell, which at 11N is topographically restricted

Table 4. Estimates of the meridional overturning cell in the Atlantic Ocean, defined as the total NADW plus AABW transport, or equivalently the net transport below roughly 4°–5°C.

	Method	Meridional cell [Sv]
Hall & Bryden, 1982	IGY hydrography @ 24N	16
Roemmich, 1983	IGY hydrography @ 8N	21
Roemmich & Wunsch, 1985	IGY hydrography @ 24N	18†
	1981 hydrography @ 24N	18†
Roemmich & Wunsch, 1985	IGY hydrography @ 36N	12†
	1981 hydrography @ 36N	17†
Sarmiento, 1986	model results at 11N	10
Semtner & Chervin, 1988	model results at 11N	8
Rintoul, 1991	IGY hydrography @ 32S	13
Schmitz & Richardson, 1991	hydrography of Florida Straits and Caribbean passages	13
Semtner & Chervin, 1992	model results at 11N	10
Speer & Tziperman, 1992	air-sea heat and freshwater flux data	7*
Matano & Philander, 1993	model results at 30S	8

†Results shown are from reference level calculations using total transport constraints.
*From air-sea data a deep water sinking rate of 9 Sv is determined for the North Atlantic. Combining this with a typical AABW transport of 2 Sv yields an overturning rate of 7 Sv.

to the region between stations 16 and 44, or along-track distance of about 1800–3400 km.

4. Meridional transports

The horizontal circulation patterns resulting from this analysis are consistent with almost all recent current meter, float, and CTD data from the tropical North Atlantic, as described in the last section. In this section, however, we estimate a net heat flux across 11N that is significantly smaller than many previous estimates, and a freshwater flux that is slightly larger. The meridional ocean heat flux is carried by the well-known Atlantic meridional overturning cell, where warm surface waters flow northward and cold deep waters have a net southward flow. For comparison with previous studies, we define the magnitude of this exchange, which we call the meridional overturning cell, to be the net (southward) transport of cold water, $\theta < 4.7°$, comprising both the NADW and AABW transports. (Equivalently, since we have conserved mass across the 11N section, the magnitude of this cell is also equal to the net *northward* transport of warm water, $\theta > 4.7°$.) The meridional overturning cell for this section is thus 5.2 ± 1.6 Sv, as shown in Figure 6. A comparison of this value with estimates from a number of other studies (Table 4) shows that although our result supports the recent modeling and indirect estimates of Semtner and Chervin (1988, 1992), Speer and Tziperman (1992), and Matano and Philander (1993), it is only a third the size of most estimates obtained directly from hydro-

graphic IGY data. However, as discussed in Section 2, the magnitude of this cell and the associated fluxes are all sensitive to changes in the Ekman and shallow NBC transport. In the following discussion, therefore, we present meridional transports not only for the circulation of Figure 6, meant to represent March 1989, but we also estimate appropriate values for an "average" March, and for the annual average. (Additional details of this analysis can be found in Friedrichs (1993).) Annual average fluxes estimated in this way are in good agreement with other results in the tropics. Other sources of uncertainty inherent in our calculations are discussed in Section 4c.

a. Heat transport. Our analysis follows the lines of Hall and Bryden (1982) and Bryden *et al.* (1991). Total heat transport across the 11N section, H_{11}, can be expressed as the sum of three components:

$$H_{11} = H_e + H_w + H_g,$$

where H_w is the net heat transport (geostrophic plus Ekman) between the Brazil coast and the first CTD station, and H_e and H_g are the Ekman and geostrophic heat transports across the rest of the 11N section. These heat transport components must be defined relative to a specific temperature. Since we allow no net meridional mass transport across the section (Fig. 6), the total heat transport, H_{11}, will be independent of this reference temperature; however, the relative sizes of the components will depend on their specific definitions (Bryden *et al.,* 1991). Here the reference temperature is taken as the area averaged mean temperature of the section evaluated from the CTD data: $\bar{\theta} = 4.38°C$.

The Ekman heat transport component is approximated as:

$$H_e = \int\int \rho C_p(\theta_e - \bar{\theta})v_e \, dx \, dz \approx \rho C_p(\overline{\theta_e} - \bar{\theta})M_e,$$

where ρ is the density of seawater, C_p is the specific heat capacity of seawater at constant pressure, θ_e is the potential temperature within the Ekman layer, v_e is the Ekman velocity, M_e is the Ekman transport, and overbars denote mean values. As described in Section 2a, Ekman transport across the 11N section is estimated to be 9.1 ± 1.8 Sv with a mean penetration depth of roughly 100 m (Chereskin and Roemmich, 1991). The Ekman temperature $\overline{\theta_e}$ has been calculated as a velocity and area weighted average of θ over the top 100 m of the water column, and the western 3000 km of the basin (since Chereskin and Roemmich (1991, their Fig. 6) show that this is where the transport occurred during March 1989). The velocity profile used for the weighting is that associated with the component of Ekman velocity normal to the section, namely, $v(z) = e^{-z/D_E}\sin(z/D_E)$, where D_E, the Ekman depth, is about 40 m if the Ekman transport is carried in the upper 100 m. We find $\overline{\theta_e} = 23.9 \pm 0.6°C$ but since including the eastern 1000 km would yield a value about 1°C lower, we increase the error bar to ±1.0°C. We note that errors in H_e are dominated by errors in M_e

anyway, not $\overline{\theta}_e$. Hence we obtain

$$H_e = 7.3 \pm 1.5 \times 10^{14} W.$$

Similarly, the heat transport over the western continental shelf can be approximated as:

$$H_w = \int\int \rho C_p(\theta_w - \overline{\theta}) v_w \, dx \, dz \approx \rho C_p(\overline{\theta_w} - \theta) M_w.$$

The mass transport over the shelf, M_w, was computed from the ADCP data to be 4.5 ± 1.0 Sv. Since no temperature data were taken along with the ADCP velocities on the continental shelf, temperatures from CTD station 85 were used to estimate the average temperature of this transport to be 26.5 ± 1.5°C, for a total

$$H_w = 4.1 \pm 0.9 \times 10^{14} W.$$

(The error of H_w is again dominated by the uncertainty in the transport value, not in the temperature value.)

Geostrophic heat transport is given by:

$$H_g = \int\int \rho C_p(\theta - \overline{\theta}) v \, dx \, dz = \int\int \rho C_p(\theta - \overline{\theta}) v_g \, dx \, dz + \rho C_p(\overline{\theta} - \overline{\theta}) A v_o,$$

Here $v = v_g + v_o$, where v_g is geostrophic velocity assuming the reference level is a level of no motion, v_o is the uniform velocity added to the section to conserve mass, and A represents the area of the 11N section. Because H_g is defined relative to the section averaged temperature, the term representing heat transport due to the uniform velocity v_o is identically zero. The term containing v_g, which is independent of M_e and M_w, is integrated over CTD stations 1–84 for the allowed reference level combinations, and yields a mean result of $H_g = -8.4 \pm 0.1 \times 10^{14}$ *W*.

Summing the three components H_e, H_w, and H_g yields a total heat transport across 11N of $H_{11} = 3.0 \pm 1.8 \times 10^{14}$ *W*. Since the heat flux in the Atlantic is so closely correlated with the meridional overturning, it is not surprising that this heat transport estimate is also considerably smaller than a number of previous tropical North Atlantic heat flux estimates which have typical values of $8 - 11 \times 10^{14}$ *W* (see Table 5). We must note, however, that synoptic variability—the fact that the cruise was characterized by atypically light March winds—will have a significant impact on the estimated March heat flux. If we were to base our calculations on the climatological March value of Ekman transport (13.5 versus 9.1 Sv), and use $\overline{\theta}_e = 22.8$°C based on the full 4000 km, the magnitude of the overturning cell increases to 8.4 Sv, and the associated heat flux approximately doubles, to 5.9×10^{14} *W* (Table 6).

It is also important to note that the values in Table 5 represent annual average estimates, whereas our estimates are for March. Seasonal changes in air-sea fluxes imply accompanying changes in oceanic transports of heat and freshwater, which may be significant relative to the annual averages. For instance, at 24N, where annual

Table 5. Annual average heat transport estimates [10^{14} W] across 10–11N in the Atlantic.

Bunker, 1976*	8
Lamb, 1981*	11
Wunsch, 1984†	1–12
Russell *et al.,* 1985‡	14
Hsiung, 1985*	8
Sarmiento, 1986‡	8
Philander & Pacanowski, 1986b‡	10
Semtner & Chervin, 1992‡	8

*surface heat budget.
†data.
‡model.

average meridional heat flux attains its maximum value in the Atlantic, values range from 6.9×10^{14} *W* in February to 18.6×10^{14} *W* in July (Molinari *et al.,* 1990). Ekman and western boundary current transports vary even more dramatically in the tropics than in the mid-latitudes, and the greatest seasonal change in Ekman transport occurs at roughly 5–10N, with a maximum from January to March, and a minimum from August to October (Isemer and Hasse, 1987). The seasonal variability of the NBC is even greater: Recent studies of the NBC indicate that the total transport of this current may range from roughly 10 Sv in the spring, to 30–35 Sv in the fall (Philander and Pacanowski, 1986a; Johns *et al.,* 1992).

In view of these strong seasonal cycles characteristic of the tropical Atlantic circulation, one might anticipate heat (and freshwater) flux variability at 11N to be at least as large as that in the mid-latitudes. In order to obtain estimates of the annual average fluxes across 11N, our geostrophic transport can be forced to balance the sum of the annual average Ekman transport (approximately 10 Sv) and the shallow NBC transport. Since the annual average total NBC transport is roughly 20 Sv, and 7 Sv were found using the CTD data offshore of the 200 m isobath (assumed to be seasonally independent for the purpose of this computation), the annual average shallow (< 200 m) NBC transport is taken to be 13 Sv. Choosing appropriate annual average values for $\overline{\theta_e}$ and $\overline{\theta_w}$ is difficult, since temperature and transport variability could be correlated. However, rough estimates based on annual average values from

Table 6. Meridional volume, heat, and freshwater fluxes across 11N for the three methods of balancing net mass for the section (see text). For each case, the sum of the Ekman and shallow NBC transports is indicated in parentheses.

Mass balance method (Ekman & NBC)	Overturning cell (Sv)	Heat flux (10^{14} W)	Freshwater flux (Sv)
March 1989 (13.6 Sv)	5.2	3.0	−0.65
March Climatology (18.0 Sv)	8.4	5.9	−0.75
Annual Average (23 Sv)	12	11	−0.6

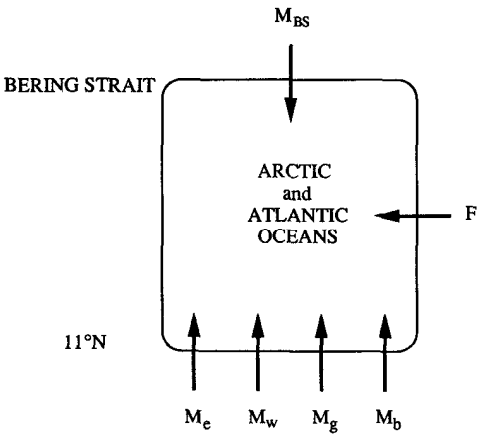

Figure 11. Mass balance for the region between the Bering Strait and the 11N section: F = net gain of freshwater integrated from the Bering Strait to 11N, M_e = Ekman mass transport, M_w = shallow western boundary mass transport, M_g = geostrophic mass transport, M_b = barotropic mass transport, M_{BS} = mass transport entering the Atlantic via the Bering Strait.

atlases ($\overline{\theta_e}$ = 23.8°C, $\overline{\theta_w}$ = 26.1°C; Robinson *et al.,* 1979; Isemer and Hasse, 1987), combined with the above transport estimates, yield an annual average meridional overturning cell of 12 Sv, and an annual average heat flux of 11 × 10^{14} *W* (Table 6). These respective values agree well with the volume transports of Table 4 and the annual average heat fluxes of Table 5. Altering either $\overline{\theta_e}$ or $\overline{\theta_w}$ by 1.0°C changes this heat flux only by about 0.5 × 10^{14} *W* (assuming our M_e and M_w estimates are correct); however, with $\overline{\theta_e}$ and $\overline{\theta_w}$ fixed, a 2 Sv error in either M_e or M_w changes H_{11} by 1.5–2.5 × 10^{14} *W*. Before discussing other possible sources of uncertainty in these estimates, we turn to the freshwater transport.

b. Freshwater transport. Freshwater transport, defined as the component of seawater flux that is pure water, can be determined by means of mass and salt conservation equations. As shown below, these equations represent the mass and salt balances for the region including both the Arctic and the Atlantic Oceans, and are illustrated schematically in Figure 11.

We express mass conservation with this equation:

$$0 = \rho M_{BS} + F + \rho M_e + \rho M_w + \rho M_g + \rho M_b.$$

In our previous volume and heat transport calculations, the North Atlantic was treated as a closed basin with the net mass transport across 11N assumed to be identically zero. However, the flow entering the Atlantic via the Bering Strait, M_{BS}, must be considered when balancing freshwater. Coachman and Aagaard (1988) find the magnitude of this throughflow to be 0.8 ± 0.1 Sv. The net gain of freshwater (i.e., precipitation minus evaporation plus land runoff) integrated from the Bering Strait

to 11N in the Atlantic is denoted F, and is one of the two unknowns in the above equation. The Ekman, western boundary, and geostrophic components of northward mass transport across 11N are represented by M_e, M_w, and M_g respectively. As discussed in Section 2, M_g has been defined to balance exactly the sum of M_e and M_w:

$$M_g = \int\int (v_g + v_o)\, dx\, dz = -(M_e + M_w).$$

To allow for the possibility that the net transport across the section is not identically zero (i.e., M_{BS} need not balance F exactly) a small unknown barotropic component of mass transport across 11N, M_b, has been included in the mass conservation equation. This is equivalent to acknowledging that the small evaporative mass fluxes that were negligible in the previous heat and volume transport calculations are now an important component of the freshwater transport. Our neglect of M_b until now can be justified *a posteriori* by examining the magnitude of this term. Since the value of ρ does not vary substantially from one, it will be omitted in the remaining calculations.

Salt conservation may be expressed as:

$$0 = M_{BS}\overline{S_{BS}} + M_e\overline{S_e} + M_w\overline{S_w} + M_b\overline{S} + M_g\overline{S_g}.$$

Long-term measurements indicate that the transport averaged salinity of the Bering Strait throughflow, $\overline{S_{BS}}$, is 32.5 psu (Coachman and Aagaard, 1988). The Ekman and western boundary salinities, $\overline{S_e} = 36.21 \pm .04$ and $\overline{S_w} = 36.21 \pm 0.10$ are computed in the same manner as $\overline{\theta_e}$ and $\overline{\theta_w}$ were determined in the previous section. The area averaged salinity for the 11N section is denoted by $\overline{S} = 34.95$ psu, while the transport averaged salinity is defined by:

$$\overline{S_g} = \frac{\int\int vS\, dx\, dz}{M_g} = 36.37 \pm 0.02 \text{ psu}.$$

Combining the mass and salt conservation equations and solving for F yields a value $F = -0.12$ Sv. The sign of this result indicates that within this Arctic/Atlantic region net evaporation exceeds precipitation and land runoff.

The quantity we wish to determine is the freshwater transport crossing 11N, i.e. F_{11}. This can be expressed as the sum of the net gain of freshwater between the Bering Strait and 11N, F, and the freshwater transport through the Bering Strait, F_{BS}. Above we determined that $F = -0.12$ Sv, while F_{BS} is simply given by:

$$F_{BS} = M_{BS}\left(1 - \frac{\overline{S_{BS}}}{1000}\right).$$

With the sign convention of Figure 11 these three quantities must sum to zero:

$$0 = F_{11} + F + F_{BS},$$

whence we compute the freshwater transport across 11N to be $F_{11} = -0.65 \pm 0.10$ Sv.

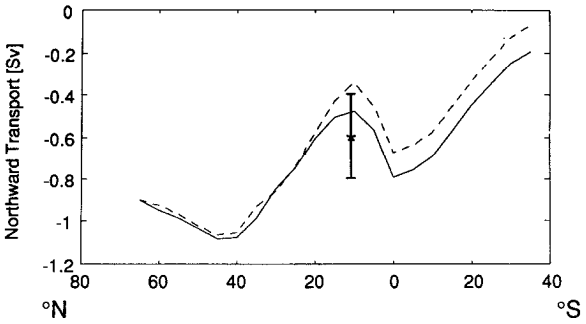

Figure 12. Indirect estimates of the northward transport of freshwater in the Atlantic Ocean as a function of latitude: integration using the data of Baumgartner and Reichel (1975) is denoted by a solid line, while that using the updated data of Schmitt *et al.* (1989) is shown by a dashed line. The asterisk denotes the annual average freshwater transport across 11N obtained from this analysis (see Table 6). [Adapted from Wjiffels *et al.*, 1992.]

Since the flow of freshwater from the Pacific into the Arctic/Atlantic system is greater than the freshwater leaving the system (via net evaporation), the net freshwater flow across 11N is southward.

Following our approach for the heat fluxes above, we compute values of freshwater transport for a climatological average March (using $\overline{S_e} = 36.08$) as well as the annual average ($\overline{S_e} = 35.76$, $\overline{S_w} = 35.6$), and include these in Table 6. Since within the North Atlantic March is typically a month of lower than average evaporation and higher than average precipitation (Isemer and Hasse, 1987), it is not surprising that the climatological March estimate of southward freshwater flux (0.75 Sv) exceeds our estimate for the annual average (0.6 Sv). Note that these freshwater fluxes are more sensitive to errors in the choice of $\overline{S_e}$ and $\overline{S_w}$, and less sensitive to errors in M_e and M_w, than the corresponding heat fluxes. Changes of the salinities by 0.5 psu lead to $\Delta F_{11} = 0.1$–0.2 Sv, while changes of 5–10 Sv in M_e or M_w would be required to affect the value of F_{11} by that same amount.

Freshwater fluxes have been computed indirectly using North Atlantic values of air-sea freshwater exchange and land runoff. Wijffels *et al.* (1992) integrate these data, presented both by Baumgartner and Reichel (1975, Table 35) and more recently by Schmitt *et al.* (1989), southward from 65N. As a northern boundary value they use the sum of the freshwater transport of the Bering Strait and the precipitation and runoff over the Arctic Ocean. Results of their analysis appear in Figure 12, along with our annual estimate from Table 6; the error bar indicates ±0.2 Sv. Our direct calculation of F_{11} suggests that there may be a greater southward flux of freshwater across 11N than has been deduced indirectly from air-sea exchanges and runoff.

c. Sources of uncertainty. The qualitative features of the deep and bottom water circulation patterns illustrated in Figure 10 are basically insensitive to the size of the

Ekman and shallow NBC transports which the geostrophic transports are required to balance. This robustness results from the strength of the ubiquitous recirculation cells relative to imposed changes in net meridional transports. For example, increasing the sum of the Ekman and shallow NBC transports by 9.4 Sv (the difference between March 1989 and annual average values) leads to an increased net southward transport of lower NADW in the eastern basin of about 2.3 Sv, compared to the recirculation cell there with a strength of 6 Sv. The middle NADW gyre in the eastern basin is most sensitive to the change: its net northward throughflow would be reduced by 1.4 Sv. In contrast, heat and freshwater fluxes are demonstrably sensitive to the strongly seasonal Ekman and shallow NBC transports, as well as other sources of uncertainty. These include methodology of the calculation itself, data resolution, and temporal changes in baroclinicity. We briefly review these other uncertainties and indicate their potential impact on the net overturning cell.

First, consider the methodology. As was evident from Figure 3, a single reference level for the entire section could not produce adequate transport results. However, one might ask why limit the number of reference level regions to four? By taking this simple approach, we hoped the analysis method would not obscure the results. In order to determine whether this was the case, the eastern basin, formerly considered as a whole, was divided into three separate regions. Western basin reference levels were kept the same as in the above analysis, since the good quantitative agreement we obtain in the western basin suggests that the flow there is represented well by our reference level choices. Reference levels in each of the three regions of the eastern basin were examined between 1000 db and 4500 db, by 500 db increments, for all possible combinations. Since two more unknowns were added to the system, two additional constraints were also imposed: (a) the transport of $\theta < 2.0°C$ across the eastern basin must be between 1 and 3 Sv northward (McCartney *et al.,* 1991), and (b) the transport of $2.0° < \theta < 2.7°C$ across the eastern basin must be at least 0.5 Sv northward. (We feel the latter constraint is a reasonable one, since Warren and Speer (1991) have found 1.8 Sv within this approximate temperature class flowing northward across 11S.) When these constraints are satisfied, the maximum possible meridional overturning cell is only 6 Sv, which is still considerably lower than the other estimates of Table 4. This result suggests that the relatively low net meridional volume and heat fluxes obtained here are not artifacts of our specific choice of reference level regions.

The relatively coarse vertical and horizontal resolution of the IGY data may be another explanation as to why the estimates based on the IGY hydrographic data are greater than most of the other estimates shown in Table 4. Beneath 2000 m, IGY measurements were spaced vertically by 200–300 m. Furthermore, typical mid-ocean station spacing of the IGY data was roughly 200 km, in contrast to the nominal 50 km spacing (10–25 km over steep topography) used in this study. Not only was the western boundary current frequently not resolved, but as noted by Roemmich and

Wunsch (1985), such low horizontal resolution can be problematic if mesoscale features are aliased into longer wavelengths and are mistaken as gyre-scale components of the general circulation. Subsampling the 1989 11N dataset at IGY resolution and repeating our calculation yields a meridional overturning cell of up to 10.3 Sv, or using the climatological Ekman transport in place of the *in situ* value, up to 13.5 Sv. Thus, much of the apparent discrepancy between our result and the other direct results listed in Table 4 may be due to the coarse resolution of the IGY data.

Temporal changes in baroclinicity will also affect net transport calculations. It is possible that on decadal time scales the baroclinic structure of the deep and bottom waters may change due to variability in the production rate of their source waters. Indeed, such change has been documented at 24 and 36N by Roemmich and Wunsch (1985), who found evidence for decreasing middle NADW production between 1957 and 1981. It is difficult to say with certainty how long a change in source water production in the North Atlantic would take to propagate to the tropics without knowing average water parcel speeds throughout the DWBC, and more details of the linkages between the boundary current and interior flows. However, Roemmich and Wunsch found that meridional heat transport at 24 and 36N was relatively insensitive to the observed change in deep baroclinic structure. Hence, we suspect that the other effects described above would tend to swamp the decadal (and longer time scale) signal at 11N.

On shorter time scales, we note that implicit in the computation of an annual average overturning cell is the assumption that the baroclinic component of the mid-ocean geostrophic velocity field is seasonally independent. In this region the increasing strength of the NBC is usually associated with an offshore increase in the southeastward flowing NECC (Richardson and Walsh, 1986), resulting in a constant net flow for the combined NBC and NECC system (Csanady, 1985). Although we adjusted the shallow NBC transport for our annual average estimates in Sections 4a and 4b, we did not account explicitly for this increase in the southeastward flowing NECC. However, Katz (1993) has documented that in March 1989 the NECC was present with an uncommonly large transport (for March) of nearly 14 Sv, which coincidently is comparable to the annual average NECC transport estimated from the values he presents for the years 1983–1989. Since this NECC transport is most likely already included in our geostrophic velocities, our annual average estimates (Table 4) are fortuitously more representative than one might have supposed. Furthermore, this unusual March appearance of the NECC may explain why our March 1989 value (3×10^{14} *W*) is so much lower than that estimated by Hsiung *et al.* (1989) from surface heat budgets (17×10^{14} *W*).

5. Summary

The net meridional transports of volume, heat and freshwater across 11N during March 1989, as computed from our results, depart significantly from historical and

numerically modeled values for these fluxes. Although a number of sources of uncertainty are present in this calculation, this discrepancy is most likely due to the atypically light winds as well as to the unusual appearance of the NECC in March 1989. Applying annual estimates of the Ekman and shallow NBC transports, and furthermore assuming that the baroclinic component of the mid-ocean geostrophic velocity field is seasonally independent (a relatively strong assumption due to the fortuitous appearance of the NECC in March 1989), we can compute annual average estimates of these fluxes. The corresponding overturning cell (12 Sv), heat flux (11×10^{14} *W*), and freshwater flux (−0.6 Sv) are all consistent with previous results.

Despite the sources of uncertainty affecting the net meridional volume, heat and freshwater transports, we reassert the robustness of the horizontal circulation patterns proposed in Section 3. Although we have emphasized the circulation of deep and bottom waters, a brief overview of the circulation of four shallow water masses was presented as well. The NBC was found to flow northwestward along the western boundary with a transport of nearly 12 Sv for $\theta > 12°C$. Southward counterflow (−25 Sv for $\theta > 7°C$) located just offshore of the NBC may have indicated the presence of the NECC, observed by Katz (1993) to be present in March 1989. The remainder of the section was characterized by primarily northward flow over the western flank of the MAR, southward flow over the eastern flank, and a small net northward flow in the eastern basin. Transports of these water masses support the results of Schmitz and Richardson (1991) who found that nearly half of the Florida Current waters are derived from the South Atlantic.

Schematic circulation patterns for four deep water masses (upper NADW, middle NADW, lower NADW, and AABW) have been presented and discussed in detail. To obtain these, we have synthesized the results from a CTD/ADCP section nominally located at 11N with other quantitative and qualitative knowledge of low latitude tropical circulation in the North Atlantic. Within the tropical North Atlantic, this study confirms the presence (and quantifies the strength) of a cyclonic recirculation gyre in the western basin, whose existence has been suggested by recent low latitude studies primarily on the basis of water property signatures. This gyre consists of the DWBC in the west, carrying 26.5 Sv southward, and a return northward flow almost half this size along the western flank of the MAR. The AABW and the upper and lower NADW cores participate in this gyre. Although there is a large 5 Sv northward flow of middle NADW banked up against the western flank of the MAR, this is believed to be a separate current derived from the South Atlantic; it is unclear to what extent, if any, the middle NADW is recirculating. In the DWBC itself, the upper and middle NADW cores are banked up against the western boundary, while the flow of lower NADW is farther offshore and considerably wider.

The eastern basin is also characterized by a cyclonic gyre, strongest in the lower NADW, and supplemented by middle NADW and AABW, and is associated with a net northward flow uniformly distributed in depth. If we suppose that this northward

flow in the eastern basin is driven dynamically by a stretching of the deep water column at the bottom of the thermocline, we can calculate maximum upwelling velocity at the top of the upper NADW of

$$w = \frac{\beta \int\int v \, dy \, dz}{f \int\int dy \, dz} = O(10^{-5} \text{ cm s}^{-1})$$

which is consistent with expected upwelling velocities in a Stommel-Arons model of the deep flow.

Although studies of the deep circulation have been carried out south of the equator as well, it is still unclear how the flow is connected crossing the equator. From a descriptive point of view, direct velocity measurements made by floats or current meters will be required within a few degrees of the equator (where the geostrophic relation breaks down) to resolve paths of water parcels as they go from the North to the South Atlantic and vice versa. Richardson and Schmitz's recent (1993) float study has begun to elucidate this issue, as does work in progress with M. McCartney (Friedrichs *et al.,* 1993) which includes a comparison of sections both north and south of the equator. As part of the WOCE Deep Basin Experiment, an intensive observational program is underway in the Brazil Basin, which lies west of the MAR between 32S and 4N. One of the objectives of this experiment is to investigate how deep water crosses the equator. As the Deep Basin Experiment data become available, they will complement the extensive suite of STACS observations to the north, and the float data of Richardson and Schmitz, in order to paint a dynamically more complete picture of the deep circulation in the western tropical Atlantic.

Acknowledgments. Support for this research was provided by grants OCE-8716314 and OCE-9101636 from the National Science Foundation, and a graduate student fellowship from the Office of Naval Research through the American Society for Engineering Education. We would like to thank Teri Chereskin and Dean Roemmich for their help in determining the boundary current and Ekman transports. Mike McCartney has generously shared many preliminary results with us regarding details of the deep tropical Atlantic circulation, which were useful in closing the schematic circulations of Figure 10. This is Woods Hole Oceanographic contribution number 8346.

REFERENCES

Amos, A. F., A. L. Gordon and E. D. Schneider. 1971. Water masses and circulation patterns in the region of the Blake-Bahama Outer Ridge. Deep-Sea Res., *18,* 145–166.

Barrett, J. R. 1965. Subsurface currents off Cape Hatteras. Deep-Sea Res., *12,* 173–184.

Baumgartner, A. and E. Reichel. 1975. The World Water Balance. Elsevier, 179 pp.

Bryden, H. L., D. H. Roemmich and J. A. Church. 1991. Ocean heat transport. Deep-Sea Res., *38,* 297–324.

Bunker, A. F. 1976. Computations of surface energy flux and annual air-sea interaction cycles of the North Atlantic Ocean. Mon. Wea. Rev., *104,* 1122–1140.

Candela, J., R. C. Beardsley and R. Limeburner. 1992. Separation of tidal and subtidal currents in ship-mounted acoustic doppler current profiler observations. J. Geophys. Res., *97,* 769–788.

Chereskin, T. K. and D. Roemmich. 1991. A comparison of measured and wind-derived Ekman transport at 11°N in the Atlantic Ocean. J. Phys. Oceanogr., *21,* 869–878.

Coachman, L. K. and K. Aagaard. 1988. Transports through Bering Strait: Annual and interannual variability. J. Geophys. Res., *93,* 15535–15539.

Csanady, G. T. 1985. A zero potential vorticity model of the North Brazilian Coastal Current. J. Mar. Res., *43,* 553–579.

Fine, R. A. and R. L. Molinari. 1988. A continuous deep western boundary current between Abaco (26.5N) and Barbados (13N). Deep-Sea Res., *35,* 1441–1450.

Friedrichs, M. A. M. 1993. Meridional Circulation in the Tropical North Atlantic. Woods Hole Oceanographic Institution Technical Report, WHOI-93-06.

Friedrichs, M. A. M., M. S. McCartney and M. M. Hall. 1993. Hemispheric asymmetry of deep water transport modes in the Atlantic. J. Geophys. Res. (submitted).

Fuglister, F. C. 1957. Oceanographic data from Crawford cruise ten obtained for the International Geophysical Year 1957–1958. Woods Hole Oceanographic Institution Technical Report, 57–54.

Georgi, D. T. and J. M. Toole. 1982. The Antarctic Circumpolar Current and the oceanic heat and freshwater budgets. J. Mar. Res., *40*(Suppl.), 183–195.

Hall, M. M. and H. L. Bryden. 1982. Direct estimates and mechanisms of ocean heat transport. Deep-Sea Res., *29,* 339–359.

Hellerman, S. and M. Rosenstein. 1983. Normal monthly wind stress over the world ocean with error estimates. J. Phys. Oceanogr., *13,* 1093–1104.

Hsiung, J. 1985. Estimates of global oceanic meridional transport. J. Phys. Oceanogr., *15,* 1405–1413.

Hsiung, J., R. E. Newell and T. Houghtby. 1989. The annual cycle of oceanic heat storage and oceanic meridional heat transport. Q. J. R. Meteorol. Soc., *115,* 1–28.

Isemer, H. J. and L. Hasse. 1987. The Bunker Climate Atlas of the North Atlantic Ocean. Springer-Verlag, 252 pp.

Johns, W. E., D. M. Fratantoni and R. J. Zantopp. 1993. Deep Western Boundary Current variability off Northeastern Brazil. Deep-Sea Res., *40,* 293–310.

Johns, W. E., T. N. Lee, F. A. Schott, R. J. Zantopp and R. Evans. 1990. The North Brazil Current Retroflection: seasonal structure and eddy variability. J. Geophys. Res., *95,* 22103–22120.

Johns, W. E., T. N. Lee and R. J. Zantopp. 1992. Seasonal Cycle and Variability of the North Brazil Current at 4N in the Tropical Atlantic. Eos, Trans. Amer. Geophys. Union, *72* (Suppl.), 21 (abstract).

Katz, E. J. 1993. An interannual study of the Atlantic North Equatorial Countercurrent. J. Phys. Oceanogr., *14,* 116–123.

Lai, D. Y. 1984. Mean flow and variabilities in the deep western boundary current. J. Phys. Oceanogr., *23,* 1488–1498.

Lamb, P. J. 1981. Estimates of annual variation of Atlantic Ocean heat transport. Nat., *290,* 766–768.

Leaman, K. D. and J. E. Harris. 1990. On the average absolute transport of the deep western boundary currents east of Abaco Island, the Bahamas. J. Phys. Oceanogr., *20,* 467–475.

Lee, T. N., W. Johns, F. Schott and R. Zantopp. 1990. Western boundary current structure and variability east of Abaco, Bahamas at 26.5N. J. Phys. Oceanogr., *20,* 446–466.

Matano, R. P., and S. G. H. Philander. 1993. Heat and mass balances of the South Atlantic Ocean calculated from a numerical model. J. Geophys. Res., *98,* 977–984.

McCartney, M. S. 1993. Crossing of the equator by the deep western boundary current in the western Atlantic Ocean. J. Phys. Oceanogr., *23,* 1953–1974.

McCartney, M. S., S. L. Bennett and M. E. Woodgate-Jones. 1991. Eastward flow through the Mid-Atlantic Ridge at 11N and its influence on the abyss of the eastern basin. J. Phys. Oceanogr., *21,* 1089–1121.

McCartney, M. S. and R. Curry. 1993. Transequatorial flow of Antarctic bottom water in the western Atlantic Ocean: abyssal geostrophy at the equator. J. Phys. Oceanogr., *23,* 1264–1276.

Molinari, R. L., R. A. Fine and E. Johns. 1992. The Deep Western Boundary Current in the tropical North Atlantic Ocean. Deep-Sea Res., *39,* 1967–1984.

Molinari, R. L., E. Johns and J. F. Festa. 1990. The annual cycle of meridional heat flux in the Atlantic Ocean at 26.5N. J. Phys. Oceanogr., *20,* 476–482.

Philander, S. G. H. and R. C. Pacanowski. 1986a. A model of the seasonal cycle in the tropical Atlantic Ocean. J. Geophys. Res., *91,* 14192–14206.

—— 1986b. The mass and heat budget in a model of the tropical Atlantic Ocean. J. Geophys. Res., *91,* 14212–14220.

Richardson, P. L. 1977. On the crossover between the Gulf Stream and western boundary undercurrent. Deep-Sea Res., *24,* 139–159.

Richardson, P. L. and W. J. Schmitz Jr. 1993. Deep cross-equatorial flow in the Atlantic measured with SOFAR floats. J. Geophys. Res., *98,* 8371–8387.

Richardson, P. L. and D. Walsh. 1986. Mapping climatological seasonal variations of surface currents in the tropical Atlantic using ship drifts. J. Geophys. Res., *91,* 10537–14550.

Rintoul, S. R. 1991. South Atlantic interbasin exchange. J. Geophys. Res., *96,* 2675–2692.

Robinson, M. K., R. A. Bauer and E. H. Schroeder. 1979. Atlas of North Atlantic-Indian Ocean monthly mean temperatures and mean salinities of the surface layer. U. S. Naval Oceanographic Office.

Roemmich, D. 1983. The balance of geostrophic and Ekman transports in the tropical Atlantic Ocean. J. Phys. Oceanogr., *13,* 1534–1539.

Roemmich, D. and C. Wunsch. 1985. Two transatlantic sections: meridional circulation and heat flux in the subtropical North Atlantic Ocean. Deep-Sea Res., *32,* 619–664.

Russell, G. L., J. R. Miller and L. C. Tsang. 1985. Seasonal oceanic heat transports computed from an atmospheric model. Dyn. Atmos. Oceans, *9,* 253–271.

Sarmiento, J. L. 1986. On the north and tropical Atlantic heat balance. J. Geophys. Res., *91,* 11677–11689.

Schmitt, R. W., P. S. Bogden and C. E. Dorman. 1989. Evaporation minus precipitation and density fluxes for the North Atlantic. J. Phys. Oceanogr., *19,* 1208–1221.

Schmitz, W. J., Jr. and M. S. McCartney. 1993. On the North Atlantic circulation. Rev. Geophys., *31,* 29–49.

Schmitz, W. J., Jr. and P. L. Richardson. 1991. On the sources of the Florida Current. Deep-Sea Res., *38*(Suppl.), S379–S409.

Schott, F., J. Fischer, J. Reppin and U. Send. 1993. On mean and seasonal currents and transports at the western boundary of the equatorial Atlantic. J. Geophys. Res., (in press).

Semtner, A. J. and R. M. Chervin. 1988. A simulation of the global ocean circulation with resolved eddies. J. Geophys. Res., *93,* 15502–15522.

—— 1992. Ocean general circulation from a global eddy-resolving model. J. Geophys. Res., *97,* 5493–5550.

Speer, K. G. and M. S. McCartney. 1991. Tracing lower North Atlantic deep water across the equator. J. Geophys. Res., *96,* 20443–20448.

Speer, K. and E. Tziperman. 1992. Rates of water mass formation in the North Atlantic Ocean. J. Phys. Oceanogr., *22,* 93–104.

Stommel, H. and A. B. Arons. 1960. On the abyssal circulation of the world ocean-II. An idealized model of the recirculation pattern and amplitude in oceanic basins. Deep-Sea Res., *6,* 217–233.

Swallow, J. C. and L. V. Worthington. 1961. An observation of a deep counter-current in the western North Atlantic. Deep-Sea Res., *8,* 1–9.

Warren, B. A. and K. G. Speer. 1991. Deep circulation in the eastern South Atlantic Ocean. Deep-Sea Res., *38* (Suppl.), S281–S322.

Whitehead, J. A. and L. V. Worthington. 1982. The flux and mixing rates of Antarctic Bottom water within the North Atlantic. J. Geophys. Res., *87,* 7903–7924.

Wijffels, S., H. Bryden, R. Schmitt and A. Stigebrandt. 1992. On the transport of freshwater by the oceans. J. Phys. Oceanogr., *22,* 155–162.

Wright, W. R. 1969. Deep water movement in the western Atlantic as determined by use of a box model. Deep-Sea Res., *16* (Suppl.), 433–446.

—— 1970. Northward transport of Antarctic Bottom Water in the western Atlantic Ocean. Deep-Sea Res., *17,* 367–371.

Wunsch, C. 1984. An eclectic Atlantic Ocean circulation model. Part I: the meridional flux of heat. J. Phys. Oceanogr., *14,* 1712–1733.

Wust, G. 1935. The Stratosphere of the Atlantic Ocean. Amerind Publishing, 112 pp.

—— 1955. Stromgeschwindigkeiten im Tiefen und Bodenwasser des Atlantischen Ozeans auf Grund dynamischer Berechnung der *Meteor* Profile der Deutschen Atlantischen Expedition 1925/27. Deep-Sea Res., *3* (Suppl.), 373–397.

Received: *23 March, 1993;* revised: *25 July, 1993.*